

Chapter 2

Vertically Integrated Non-hydrostatic Free Surface Flow Equations

Roman Symbols

a	Shallow water wave celerity based on enhanced gravity (m/s)
A	Finite volume area (m ²)
CFL	Courant–Friedrichs–Lewy number (–)
D	Representative particle diameter (m)
f	Weighting function (m)
\mathbf{F}	Vector of fluxes in x -direction (m ² /s, m ³ /s ²)
$\mathbf{F}_{i+1/2}$	Numerical flux in x -direction at cell interface (m ² /s, m ³ /s ²)
g	Gravity acceleration (m/s ²)
g'	Enhanced gravity acceleration (m/s ²)
\mathbf{G}	Vector of fluxes in y -direction (m ² /s, m ³ /s ²)
h	Vertical flow depth (m)
h^*	Flow depth at star region in HLL Riemann solver (m)
H	Vertical length scale (m)
i	x -index for finite volume cell (–)
I	Auxiliary variable (m ² /s)
k	Time index (–)
K	Fawer exponent (–)
L	Horizontal length scale (m)
M	Momentum function (m ²)
n	Curvilinear coordinate normal to channel bottom (m) also bed porosity (–)
N	Flow depth normal to channel bottom (m)
p	Fluid pressure (N/m ²)
p_1	Bottom pressure in excess of hydrostatic pressure (N/m ²)
p_2	Midpressure in excess of pressure average at bottom and surface elevation (N/m ²)
q	Unit discharge (m ² /s)
q_b	Unit bed load (m ² /s)
q_x	Unit discharge in x -direction (m ² /s)
q_y	Unit discharge in y -direction (m ² /s)
q_K	Signal speed factor in HLL solver (–)
R	Submerged specific gravity (–)
R_{ep}	Particle Reynolds number (–)

s	Curvilinear coordinate along channel bed (m)
S_o	Bottom slope (–)
S_f	Friction slope (–)
S_L	Speed of left signal in HLL Riemann solver (m/s)
S_R	Speed of right signal in HLL Riemann solver (m/s)
\mathbf{S}	Vector of source terms (m/s, m ² /s ²)
t	Time (s)
T_{ij}	Depth-averaged Reynolds stress (N/m ²) with $(i, j) = (x, y)$
\mathbf{T}	Stress tensor (N/m ²)
u	Velocity in x -direction (m/s)
\mathbf{u}	Depth-averaged velocity vector (m/s, m/s)
u_1	Velocity at surface in excess of mean (m/s)
U	Depth-averaged flow velocity in x -direction (m/s)
\mathbf{U}	Vector of conserved variables (m, m ² /s)
v	Velocity in y -direction (m/s)
V	Depth-averaged flow velocity in y -direction also modulus of velocity (m/s)
w	Velocity in z -direction (m/s)
\bar{w}	Depth-averaged flow velocity in z -direction (m/s)
w_2	Middepth vertical velocity in excess of average (m/s)
x	Horizontal coordinate (m)
y	Horizontal coordinate normal to x (m)
z	Vertical coordinate (m)
z_b	Bed elevation (m)

Greek Symbols

γ	Specific weight of water (N/m ³)
γ_s	Specific weight of solids (N/m ³)
ε	Shallowness parameter (–)
η	Vertical distance above channel bottom (m)
θ	Angle of bottom with horizontal (rad)
κ	Streamline curvature (m ^{–1})
$\bar{\kappa}$	Depth-averaged streamline curvature (m ^{–1})
λ	Dispersive factor (–)
ν	Kinematic viscosity (m ² /s)
ρ	Density (kg/m ³)
σ_{ij}	Turbulent Reynolds stress, with $(i, j) = (x, y, z)$ (N/m ²)
τ_b	Boundary shear stress along bed in s -direction (N/m ²)
τ_{ij}	Stress in continuum medium, with $(i, j) = (x, y, z)$ (N/m ²)
ω	Weighting parameter (–)
Ω	Control volume (m ³)

Subscripts

- s Relative to free surface
- b Relative to bottom
- L Relative to left state in Riemann problem
- R Relative to right state in Riemann problem

Superscripts

- * Relative to dimensionless quantity

2.1 Introduction

Practically, all gravity-driven flow models constitute the lowest order approximations of shallow flows, in which the horizontal length scales $[L]$ are substantially larger than the vertical length scales $[H]$ (Steffler and Jin 1993). The non-dimensional mass and momentum balance equations based on this anisotropic scaling indicate for basically horizontal flow that the vertical acceleration terms are small, with the aspect ratio $\varepsilon = [H]/[L] \rightarrow 0$, so that the vertical force balance is usually expressed as a hydrostatic pressure balance (Saint-Venant 1871; Friedrichs 1948; Liggett 1994). For a value of ε different from zero, the analogous scale analysis shows that the vertical acceleration term is important (Liggett 1994). In this case, the full vertical momentum equation must be preserved. This type of model is referred to as *Boussinesq-type model*, representing a vertically integrated system of conservation equations based on a finite ε value. It accounts for cases for which non-hydrostatic pressure distributions are relevant, including flows in hydraulic structures, sand waves in water–sediment flows, water wave motions and seepage flows, among others.

The production of a vertically integrated system of non-hydrostatic flow equations can be set up either in Cartesian or curvilinear coordinates following terrain. In a general curvilinear coordinate setting of gravity-driven flows, three types of accelerations may arise affecting the internal stress distribution of free surface flows. The first is the acceleration due to the real forces acting on the flow. The bed-normal component of this acceleration is what makes the key effect of the Boussinesq-type model. The second, actually not a real acceleration, manifests itself as an enhanced pressure due to the Christoffel symbols of the curvilinear coordinate setting and is often simply (but not correctly) referred to as centripetal acceleration. This contribution is accounted for in the well-known Dressler (1978) equations for open-channel flow. The third are the Coriolis, centripetal, and Euler accelerations because the earth-fixed frame is not inertial, routinely neglected in local shallow flow computations, but accounted for in many meteorological applications. The use of curvilinear coordinates increases the mathematical complexities of equations, so

that vertically integrated equations in a Cartesian system are used here to produce a non-hydrostatic system of conservation laws.

In the pioneering works of Boussinesq (1872, 1877) the non-hydrostatic effect was accounted for in a depth-averaged model formulated in a curvilinear setting, but Christoffel symbols were neglected (Castro-Orgaz and Hager 2011a). Serre (1953) and Castro-Orgaz and Hager (2011b) proposed a rigorous depth-averaged turbulent Boussinesq-type model for practical applications to both steady and unsteady water flows on sloping, straight-bottomed channels. Benjamin and Lighthill (1954) proposed a different theoretical treatment based on a third-order expansion of the stream function in a potential flow. The Application of the Boussinesq-type theory to hydraulic engineering¹ was successful in the description of flows over weirs, undular jumps, sand waves, Favre waves, dam breaks, overfalls, and slope breaks.

Castro-Orgaz et al. (2012, 2013) demonstrated that Boussinesq-type equations also describe free surface groundwater flows. The application of the Boussinesq theory to water wave motion was pursued by Peregrine (1966, 1967, 1972), who obtained depth-integrated inviscid Boussinesq equations in two horizontal dimensions presenting thereby the first numerical solution for undular bore propagation. He initiated the use of Boussinesq-type equations in coastal engineering. This work was followed by further improvements of the analysis of the dispersive wave characteristics of the Boussinesq system, developing accurate and robust numerical schemes and including real flow features such as wave breaking, vorticity effects, and turbulence.² Nowadays, the governing equations and numerical techniques are in a stage of development involving a large variety of water wave phenomena (Kim et al. 2009; Kim and Lynett 2011; Brocchini 2013). The application of the Boussinesq-theory to granular mass flows and geophysical problems is relatively new and was developed by Denlinger and Iverson (2004), Castro-Orgaz et al. (2015), and Hutter and Castro-Orgaz (2016).

In this chapter, the vertically integrated equations of the continuum mechanical balance laws of mass and momentum are presented as evolution equations for the velocity field and stress tensor following Castro-Orgaz et al. (2015). Boussinesq-type equations are obtained from the vertically integrated equations using Serre's (1953) theory. After suitable approximate representations for the

¹Fawer (1937), Iwasa (1955, 1956), Iwasa and Kennedy (1968), Mandrup-Andersen (1975, 1978), Marchi (1963, 1992, 1993), Matthew (1963, 1991), Engelund and Hansen (1966), Basco (1983), Hager (1983), Hager and Hutter (1984a, b), Montes (1986), Berger and Carey (1998a, b), Soares-Frazão and Zech (2002), Mohapatra and Chaudhry (2004), Dewals et al. (2006), Bose and Dey (2007, 2009), Chaudhry (2008), Castro-Orgaz and Hager (2009), Denlinger and O'Connell (2008).

²Mei (1983), Antunes do Carmo et al. (1993), Nwogu (1993), Chen and Liu (1995), Wei et al. (1995), Wei and Kirby (1995), Madsen et al. (1997), Madsen and Schäffer (1998), Stansby and Zhou (1998), Chen et al. (1999, 2003), Kennedy et al. (2000), Lynett et al. (2002), Stansby (2003), Erduran et al. (2005), Musumeci et al. (2005), Lynett (2006), Chen (2006), Soares-Frazão and Guinot (2008), Mignot and Cienfuegos (2008), Kim et al. (2009), Kim and Lynett (2011), Brocchini (2013).

stress tensor, the emerging equations are applied to turbulent water flows in rivers, flows over steep slopes, water wave propagations, and flows over uneven topography. Movable beds and sediment transport are included, and suitable numerical techniques to solve unsteady and steady flow problems are discussed. Techniques to produce higher-order models are then further presented.

2.2 Vertically Integrated Equations in Continuum Mechanical Description

2.2.1 Basic Conservation Laws

Consider the flow of a continuum material of constant density ρ moving across a 3D terrain (Fig. 2.1), such as a fluidized granular mass. In a horizontal–vertical Cartesian system of reference (x, y, z) , the terrain elevation is described by the function $z = z_b(x, y)$, and the velocity components in the (x, y, z) directions are, respectively (u, v, w) . The motion is described within the framework of continuum mechanics with mass and momentum conservation equations (Savage and Hutter 1989; Iverson 1997; Andreotti et al. 2013). The mass conservation equation states

$$\frac{\partial u}{\partial x} + \frac{\partial v}{\partial y} + \frac{\partial w}{\partial z} = 0. \quad (2.1)$$

A vector field whose divergence vanishes is called solenoidal. Equation (2.1) is the mass balance for a *density-preserving* medium. This simplification is adopted

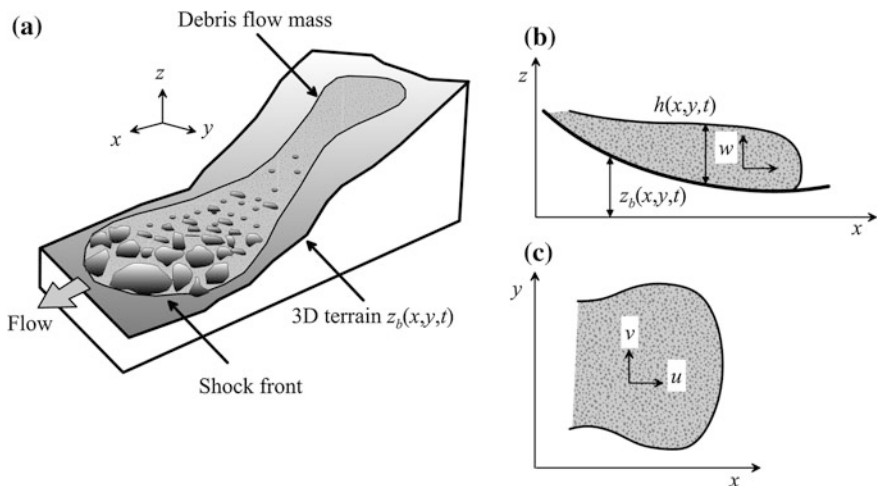


Fig. 2.1 Definition sketch for debris flow over 3D terrain **a** 3D view, **b** profile, **c** plan

here following Castro-Orgaz et al. (2015). The dynamic statement is Newton's second law, according to which the time rate of change of momentum equals the sum of the applied forces, given here by the stress divergence plus the gravity force. In horizontal-vertical Cartesian coordinates, the statement is with g as the acceleration due to gravity

$$\frac{\partial u}{\partial t} + u \frac{\partial u}{\partial x} + v \frac{\partial u}{\partial y} + w \frac{\partial u}{\partial z} = -\frac{1}{\rho} \left(\frac{\partial \tau_{xx}}{\partial x} + \frac{\partial \tau_{xy}}{\partial y} + \frac{\partial \tau_{xz}}{\partial z} \right), \quad (2.2)$$

$$\frac{\partial v}{\partial t} + u \frac{\partial v}{\partial x} + v \frac{\partial v}{\partial y} + w \frac{\partial v}{\partial z} = -\frac{1}{\rho} \left(\frac{\partial \tau_{yx}}{\partial x} + \frac{\partial \tau_{yy}}{\partial y} + \frac{\partial \tau_{yz}}{\partial z} \right), \quad (2.3)$$

$$\frac{\partial w}{\partial t} + u \frac{\partial w}{\partial x} + v \frac{\partial w}{\partial y} + w \frac{\partial w}{\partial z} = -\frac{1}{\rho} \left(\frac{\partial \tau_{zx}}{\partial x} + \frac{\partial \tau_{zy}}{\partial y} + \frac{\partial \tau_{zz}}{\partial z} \right) - g. \quad (2.4)$$

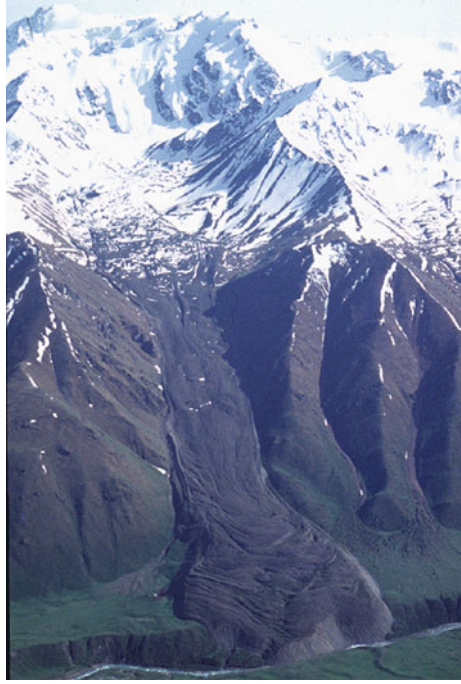
At this point, it should be noted that the stress tensor is symmetric, i.e., $\tau_{ij} = \tau_{ji}$, $ij = 1, 2, 3$, or (x, y, z) . Moreover, τ_{ij} is here introduced with the notation used in the environmental contexts (e.g., Iverson 1997, 2005; Andreotti et al. 2013), i.e., it is the negative of the common stress tensor definition used in engineering. Equations (2.1)–(2.4) define mass and momentum conservations for single constituent bodies such as water; they also apply for a dry or fluidized granular mass (Fig. 2.2), under the restricted simplification of density preserving flow.

Equations (2.2)–(2.4) relate the kinematic fields (u, v, w) to an arbitrary stress tensor \mathbf{T} . If solids are neglected and a time-averaging is performed, then \mathbf{T} would describe the stress tensor of the Reynolds-Averaged Navier-Stokes (RANS) equations (Rodi 1980), used to model turbulent water flows (Hervouet 2007; Steffler and Jin 1993; Hutter and Jöhnk 2004). Furthermore, if the fluid is absent and the stress tensor is defined based on the Mohr-Coulomb model, the equations describe the motion of a dry granular flow (e.g., Savage and Hutter 1989; Iverson 1997, 2005; Pudasaini and Hutter 2007; Andreotti et al. 2013).

The unsteady three-dimensional (3D) non-hydrostatic numerical solutions of the RANS equations for free surface flows are not a routine matter (Hervouet 2007; Ma et al. 2012). Most of the 3D numerical solutions of non-hydrostatic flows solve a pressure Poisson equation for the dynamic pressure in finite element (Hervouet 2007) or finite volume (Ma et al. 2012) models. A simplified approach to reduce computational work as compared with 3D solutions is to vertically integrate Eqs. (2.1)–(2.4) to obtain vertically averaged variables as functions of only (x, y, t) , thereby resulting in a spatially 2D computational scheme. In most practical cases, a depth-averaged computation gives enough information.³ Thus, Eqs. (2.1)–(2.4)

³Examples in hydraulic engineering were studied by Boussinesq (1877), Yen (1973), Steffler and Jin (1993), Liggett (1994), Vreugdenhil (1994), Khan and Steffler (1996a, b), Jain (2001), whereas in rapid gravity-driven mass flows the scene has been set by Hutter and Savage (1988), Savage and Hutter (1989, 1991), Iverson (1997, 2005), Denlinger and Iverson (2004). For a review, see e.g., Pudasaini and Hutter (2007).

Fig. 2.2 Glacier moraines in Tuyk Valley, Alaarcha basin North Tien Shan, Kirgizstan (from unpublished lecture material on granular media by Prof. K. Hutter, Photograph by Prof. Aizen)



provide a general starting point to produce a family of vertically integrated models within the context of continuum mechanics, valid either for water, solid particles, or (solenoidal) mixture flows.

2.2.2 *Depth-Integrated Continuity Equation*

Let the Cartesian coordinates be horizontal (x, y) and vertical (z), against gravity (Fig. 2.1). Then, the mathematical procedure consists in vertically integrating the governing equations at an arbitrary (x, y) -position from z_b to z_s , where subscripts b and s , respectively, refer to the bed and the free surface. After vertical integration, Eq. (2.1) becomes

$$\int_{z_b}^{z_s} \left(\frac{\partial u}{\partial x} + \frac{\partial v}{\partial y} + \frac{\partial w}{\partial z} \right) dz = 0. \quad (2.5)$$

Using Leibniz's rule (Yen 1973; Hutter and Jöhnk 2004), Eq. (2.5) is converted to

$$\frac{\partial}{\partial x} \int_{z_b}^{z_s} u dz - u_s \frac{\partial z_s}{\partial x} + u_b \frac{\partial z_b}{\partial x} + \frac{\partial}{\partial y} \int_{z_b}^{z_s} v dz - v_s \frac{\partial z_s}{\partial y} + v_b \frac{\partial z_b}{\partial y} + w_s - w_b = 0. \quad (2.6)$$



Joseph Valentin Boussinesq was born on March 15, 1842, at St. André-de-Sangonis, France, and passed away on February 19, 1929, in Paris. He was self-taught, starting his scientific writing in 1865. He thereby took into consideration during his long career all branches of mathematical physics except for electromagnetism. After having served as teacher at various colleges of France, he was appointed in 1873 lecturer at the University of Lille. In 1886, Boussinesq was appointed to the chair of mechanics at the famous Sorbonne University, Paris, taking over in 1896

as professor of mathematical physics at *Collège de France*.

Boussinesq's life work in hydraulics is outstanding but extremely hard to follow, given his complicated writing style. His colleagues Alfred A. Flamant (1839–1915) and Auguste Boulanger (1866–1923) were able to present in their books a more popular approach of Boussinesq's ideas. His 1872 paper explains the observations of solitary waves of John Scott Russell (1808–1882) from a physical perspective thereby overcoming the many attempts offered in the past decades. It was noted that many hydraulic phenomena could only be explained by inclusion of the streamline curvature effects. This paper particularly attracted the interest of Adhémar Barré de Saint-Venant (1797–1886), who in 1871 had published his famous paper on the shallow water equations, yet by assuming hydrostatic pressure and uniform velocity distributions. The monumental 1877 *Essay* of Boussinesq made his name definitely known to the hydraulics community given the large number of relevant problems discussed. In the 1880s, he started in addition a close collaboration with Henry Bazin (1829–1917) on weir flow features, for which streamline curvature effects again are significant. In hydraulics, this collaboration between the then best experimenter and scientist marked the start of engineering hydraulics, leading to the close relationship between scientists in mathematical physics and hydraulics in the twentieth century. The outstanding merits of Boussinesq were awarded by his nomination to the mechanics chair at Sorbonne, taking over the chair of his intimate colleague de Saint-Venant.

As to the kinematic boundary conditions, the movement of the material free surface is described by

$$\frac{\partial z_s}{\partial t} + u_s \frac{\partial z_s}{\partial x} + v_s \frac{\partial z_s}{\partial y} - w_s = 0. \quad (2.7)$$

Similarly, the kinematic equation at the movable material bed surface takes the form

$$\frac{\partial z_b}{\partial t} + u_b \frac{\partial z_b}{\partial x} + v_b \frac{\partial z_b}{\partial y} - w_b = 0, \quad (2.8)$$

where a slip velocity at the bed is allowed in depth-averaged modelling. Inserting Eqs. (2.7) and (2.8) into Eq. (2.6) produces with the vertical flow depth given by $h = h(x, y, t) = z_s(x, y, t) - z_b(x, y, t)$ (Fig. 2.1)

$$\frac{\partial h}{\partial t} + \frac{\partial q_x}{\partial x} + \frac{\partial q_y}{\partial y} = 0. \quad (2.9)$$

Equation (2.9) states the general depth-integrated mass (or here volume) conservation subjected to a density preserving body and material free and basal surfaces. The integrals in Eq. (2.9) are the fluxes q_x and q_y in the (x, y) directions given by

$$q_x = \int_{z_b}^{z_s} u dz, \quad q_y = \int_{z_b}^{z_s} v dz. \quad (2.10)$$

2.2.3 Depth-Integrated Momentum Equations in Horizontal Plane

Integrating Eq. (2.2) over the depth yields

$$\int_{z_b}^{z_s} \left(\frac{\partial u}{\partial t} + u \frac{\partial u}{\partial x} + v \frac{\partial u}{\partial y} + w \frac{\partial u}{\partial z} \right) dz = \int_{z_b}^{z_s} -\frac{1}{\rho} \left(\frac{\partial \tau_{xx}}{\partial x} + \frac{\partial \tau_{xz}}{\partial z} + \frac{\partial \tau_{xy}}{\partial y} \right) dz. \quad (2.11)$$

The acceleration term on the left-hand side of Eq. (2.11) is rewritten as

$$\frac{\partial u}{\partial t} + u \frac{\partial u}{\partial x} + v \frac{\partial u}{\partial y} + w \frac{\partial u}{\partial z} = \frac{\partial u}{\partial t} + \frac{1}{2} \frac{\partial u^2}{\partial x} + \frac{\partial(uv)}{\partial y} + \frac{\partial(uw)}{\partial z} - u \left(\frac{\partial w}{\partial z} + \frac{\partial v}{\partial y} \right), \quad (2.12)$$

or with the aid of Eq. (2.1),

$$\frac{\partial u}{\partial t} + u \frac{\partial u}{\partial x} + v \frac{\partial u}{\partial y} + w \frac{\partial u}{\partial z} = \frac{\partial u}{\partial t} + \frac{\partial u^2}{\partial x} + \frac{\partial(uv)}{\partial y} + \frac{\partial(uw)}{\partial z}. \quad (2.13)$$

Inserting Eq. (2.13) into Eq. (2.11), applying the Leibniz rule, and using Eqs. (2.7) and (2.8), the vertically integrated momentum equation in the x -direction takes the form

$$\frac{\partial}{\partial t} \int_{z_b}^{z_s} u dz + \frac{\partial}{\partial x} \int_{z_b}^{z_s} u^2 dz + \frac{\partial}{\partial y} \int_{z_b}^{z_s} uv dz = -\frac{1}{\rho} \left[\frac{\partial}{\partial x} \int_{z_b}^{z_s} \tau_{xx} dz + \frac{\partial}{\partial y} \int_{z_b}^{z_s} \tau_{xy} dz + (\tau_{xx})_b \frac{\partial z_b}{\partial x} + (\tau_{xy})_b \frac{\partial z_b}{\partial y} - (\tau_{xz})_b \right]. \quad (2.14)$$

Here, all stresses at the free surface have been assumed to vanish, that is, atmospheric pressure and wind shear stress are ignored. Likewise, the depth-integrated momentum equation in the y -direction is written as

$$\frac{\partial}{\partial t} \int_{z_b}^{z_s} v dz + \frac{\partial}{\partial y} \int_{z_b}^{z_s} v^2 dz + \frac{\partial}{\partial x} \int_{z_b}^{z_s} uv dz = -\frac{1}{\rho} \left[\frac{\partial}{\partial y} \int_{z_b}^{z_s} \tau_{yy} dz + \frac{\partial}{\partial x} \int_{z_b}^{z_s} \tau_{xy} dz + (\tau_{yy})_b \frac{\partial z_b}{\partial y} + (\tau_{xy})_b \frac{\partial z_b}{\partial x} - (\tau_{yz})_b \right]. \quad (2.15)$$

The set of Eqs. (2.14) and (2.15) describes flows with reference to the (x, y) plane. The particular case of 1D turbulent water motion in the x -direction was presented by Steffler and Jin (1993). An approximation to the kinematic field (u, v, w) and parameterizations of the stress tensor \mathbf{T} are required to produce a mathematically closed model.

2.2.4 Non-hydrostatic Stresses in z -Direction and Vertical Velocity Profile

The integration of the vertical momentum equation is similar to the deduction of the system (2.14) and (2.15). To be able to account for the non-hydrostatic stress distribution, start with the integral relation between an arbitrary elevation and the free surface; from Eq. (2.4),

$$\int_z^{z_s} \left(\frac{\partial w}{\partial t} + \frac{\partial w^2}{\partial z} + \frac{\partial(wu)}{\partial x} + \frac{\partial(wv)}{\partial y} \right) dz' = \int_z^{z_s} -\frac{1}{\rho} \left(\frac{\partial \tau_{zz}}{\partial z} + \frac{\partial \tau_{zx}}{\partial x} + \frac{\partial \tau_{zy}}{\partial y} + \rho g \right) dz'. \quad (2.16)$$

Using the Leibniz rule on the left-hand side (LHS) of Eq. (2.16) yields, after adding the free surface kinematic boundary condition given by Eq. (2.7),

$$\begin{aligned} \frac{\partial}{\partial t} \int_z^{z_s} w dz' - w_s \frac{\partial z_s}{\partial t} + \frac{\partial}{\partial x} \int_z^{z_s} w u dz' - w_s u_s \frac{\partial z_s}{\partial x} + \frac{\partial}{\partial y} \int_z^{z_s} w v dz' - w_s v_s \frac{\partial z_s}{\partial y} + w_s^2 - w^2 \\ = \frac{\partial}{\partial t} \int_z^{z_s} w dz' + \frac{\partial}{\partial x} \int_z^{z_s} w u dz' + \frac{\partial}{\partial y} \int_z^{z_s} w v dz' - w^2. \end{aligned} \quad (2.17)$$

Integrating the right-hand side (RHS) of Eq. (2.16) yields

$$\begin{aligned} \int_z^{z_s} -\frac{1}{\rho} \left(\frac{\partial \tau_{zz}}{\partial z} + \frac{\partial \tau_{zx}}{\partial x} + \frac{\partial \tau_{zy}}{\partial y} + \rho g \right) dz' = \frac{1}{\rho} [\tau_{zz}(z) - \tau_{zz}(z_s)] - g(z_s - z) \\ - \frac{1}{\rho} \int_z^{z_s} \left(\frac{\partial \tau_{zx}}{\partial x} + \frac{\partial \tau_{zy}}{\partial y} \right) dz'. \end{aligned} \quad (2.18)$$

Using the identities given by Eqs. (2.17) and (2.18) generates the general equation for the non-hydrostatic stresses as follows

$$\begin{aligned} \tau_{zz}(z) = \tau_{zz}(z_s) + \rho g(z_s - z) - \rho w^2 + \rho \frac{\partial}{\partial t} \int_z^{z_s} w dz' + \rho \frac{\partial}{\partial x} \int_z^{z_s} w u dz' + \rho \frac{\partial}{\partial y} \int_z^{z_s} w v dz' \\ + \int_z^{z_s} \left(\frac{\partial \tau_{zy}}{\partial y} + \frac{\partial \tau_{zx}}{\partial x} \right) dz'. \end{aligned} \quad (2.19)$$

As usual, a vanishing traction on the material surface implies $\tau_{zz}(z_s) = 0$. This equation describes the general distribution of τ_{zz} in the z -direction as a function of the vertical velocity w , the horizontal velocities u and v , and the indicated stresses (last term on the RHS). The equation is general allowing for a systematic development of the depth-averaged equations. By contrast, if Eq. (2.16) is integrated from $z = z_b$ to $z = z_s$, then an equation for the bed vertical normal stress is obtained

$$\begin{aligned}
(\tau_{zz})_b &= \rho gh + \rho \frac{\partial}{\partial t} \int_{z_b}^{z_s} w dz + \rho \frac{\partial}{\partial x} \int_{z_b}^{z_s} w u dz + \rho \frac{\partial}{\partial y} \int_{z_b}^{z_s} w v dz + \frac{\partial}{\partial x} \int_{z_b}^{z_s} \tau_{zx} dz \\
&+ \frac{\partial}{\partial y} \int_{z_b}^{z_s} \tau_{zy} dz + (\tau_{zx})_b \frac{\partial z_b}{\partial x} + (\tau_{zy})_b \frac{\partial z_b}{\partial y},
\end{aligned} \tag{2.20}$$

in which vanishing surface traction, implying $(\tau_{xz})_s = (\tau_{yz})_s = 0$, has been implemented. Note that the bed stress differs in general from the gravity force term (ρgh) . Deviations of $(\tau_{zz})_b$ from the static weight (ρgh) stem from streamline curvature, e.g., convective vertical acceleration terms related to $\partial w / \partial x$ and $\partial w / \partial y$, local vertical acceleration $\partial w / \partial t$, and stress contributions. Therefore, the Saint-Venant theory does not apply for steep and curved terrain.

Knowledge of the vertical velocity profile $w(z)$ is necessary in Eq. (2.20). To this end, integrating Eq. (2.1) between z_b and an arbitrary elevation z yields

$$\int_{z_b}^z \left(\frac{\partial u}{\partial x} + \frac{\partial v}{\partial y} + \frac{\partial w}{\partial z} \right) dz' = 0, \tag{2.21}$$

or

$$w(z) - w(z_b) = - \int_{z_b}^z \left(\frac{\partial u}{\partial x} + \frac{\partial v}{\partial y} \right) dz'. \tag{2.22}$$

Using again the Leibniz rule transforms this into

$$w(z) - w(z_b) = - \left[\frac{\partial}{\partial x} \int_{z_b}^z u dz' + \frac{\partial}{\partial y} \int_{z_b}^z v dz' + u_b \frac{\partial z_b}{\partial x} + v_b \frac{\partial z_b}{\partial y} \right]. \tag{2.23}$$

With the kinematic boundary condition at $z = z_b$, stated by Eq. (2.8), gives

$$w(z) = \frac{\partial z_b}{\partial t} - \left[\frac{\partial}{\partial x} \int_{z_b}^z u dz' + \frac{\partial}{\partial y} \int_{z_b}^z v dz' \right]. \tag{2.24}$$

The result for a rigid basal surface ($\partial z_b / \partial t = 0$) is, therefore,

$$w(z) = - \left[\frac{\partial}{\partial x} \int_{z_b}^z u dz' + \frac{\partial}{\partial y} \int_{z_b}^z v dz' \right]. \tag{2.25}$$

It reveals that once any functional representations for u and v are introduced, w is determined by a simple mass (volume) conservation balance. This avoids the use of an independent function of w , given that it is linked to u and v . Equation (2.25) inserted into Eq. (2.19) mathematically eliminates the dependence of τ_{zz} on w .

2.3 Shallow Flow Approximation and Depth-Averaged Equations

If the vertical thickness $h(x, y, t)$ of a nearly horizontal flow is smaller than the characteristic length in the (x, y) plane, a scaling analysis reveals that, with the exception of the near-bed boundary layer, the velocity components u and v can be assumed to be constant across the depth h , equal to their depth-averaged values U and V (Liggett 1994). Therefore,

$$u(x, y, z, t) \approx U(x, y, t) = \frac{1}{h} \int_{z_b}^{z_s} u dz, \quad (2.26)$$

$$v(x, y, z, t) \approx V(x, y, t) = \frac{1}{h} \int_{z_b}^{z_s} v dz. \quad (2.27)$$

This approach permits to obtain the non-hydrostatic equations, first derived by Serre (1953). At the limit, as the aspect ratio $\varepsilon \rightarrow 0$, the Saint-Venant hydrostatic theory is regained (Friedrichs 1948). The depth-independent horizontal velocity components imply a slip velocity at the bed, thereby neglecting the high velocity gradient confined to the thin bed boundary layer (Steffler and Jin 1993). This approximation for u and v will also be adopted for flows on steep terrain, given the small contribution of the differential advection originating from the non-uniformity of u and v with depth. Therefore, the Boussinesq velocity correction coefficients in the x - and y -directions are close to unity, so that their impact on the momentum balance projected in the corresponding axis is negligible.

Inserting Eqs. (2.26) and (2.27) into Eqs. (2.14) and (2.15) yields

$$\begin{aligned} & \frac{\partial}{\partial t}(Uh) + \frac{\partial}{\partial x}(U^2h) + \frac{\partial}{\partial y}(UVh) \\ &= -\frac{1}{\rho} \left[\frac{\partial}{\partial x} \int_{z_b}^{z_s} \tau_{xx} dz + \frac{\partial}{\partial y} \int_{z_b}^{z_s} \tau_{xy} dz + (\tau_{xx})_b \frac{\partial z_b}{\partial x} + (\tau_{xy})_b \frac{\partial z_b}{\partial y} - (\tau_{xz})_b \right], \end{aligned} \quad (2.28)$$

$$\begin{aligned}
& \frac{\partial}{\partial t}(Vh) + \frac{\partial}{\partial y}(V^2h) + \frac{\partial}{\partial x}(VUh) \\
&= -\frac{1}{\rho} \left[\frac{\partial}{\partial y} \int_{z_b}^{z_s} \tau_{yy} dz + \frac{\partial}{\partial x} \int_{z_b}^{z_s} \tau_{xy} dz + (\tau_{yy})_b \frac{\partial z_b}{\partial y} + (\tau_{xy})_b \frac{\partial z_b}{\partial x} - (\tau_{yz})_b \right]. \quad (2.29)
\end{aligned}$$

The assumption of depth-independent horizontal velocity components automatically yields for the linear vertical velocity profile, from Eq. (2.25),

$$w(x, y, z) = - \left[\frac{\partial}{\partial x} [U(z - z_b)] + \frac{\partial}{\partial y} [V(z - z_b)] \right]. \quad (2.30)$$

With $\eta = z - z_b$ and $h = z_s - z_b$, the vertical stress (pressure) in Eq. (2.19) is then given by

$$\begin{aligned}
\tau_{zz} = & \rho g(h - \eta) - \rho w^2 + \rho \frac{\partial}{\partial t} \int_z^{z_s} w dz' + \rho \frac{\partial}{\partial x} \left[U \int_z^{z_s} w dz' \right] \\
& + \rho \frac{\partial}{\partial y} \left[V \int_z^{z_s} w dz' \right] + \int_z^{z_s} \left(\frac{\partial \tau_{zy}}{\partial y} + \frac{\partial \tau_{zx}}{\partial x} \right) dz'. \quad (2.31)
\end{aligned}$$

Here, the vertical velocity field w is expressed as $w = w(U, V)$, according to Eq. (2.30).

With the definitions (2.26), (2.27), the depth-integrated mass conservation equation (2.9) takes the form

$$\frac{\partial h}{\partial t} + \frac{\partial(Uh)}{\partial x} + \frac{\partial(Vh)}{\partial y} = 0. \quad (2.32)$$

Nothing specific is yet assumed on the stress tensor \mathbf{T} , so that the system of equations applies to solids, fluids, and any other material behavior of a continuous body.

Equations (2.28), (2.29), and (2.32) can be expressed in general conservative form as

$$\frac{\partial \mathbf{U}}{\partial t} + \frac{\partial \mathbf{F}}{\partial x} + \frac{\partial \mathbf{G}}{\partial y} = \mathbf{S}, \quad (2.33)$$

in which the vector of dependent variables is \mathbf{U} , the vector of fluxes in the x -direction is \mathbf{F} , that in the y -direction is \mathbf{G} , and \mathbf{S} is the source term vector, defined by

$$\begin{aligned}
\mathbf{U} &= \begin{pmatrix} h \\ Uh \\ Vh \end{pmatrix}, \quad \mathbf{F} = \begin{pmatrix} Uh \\ U^2h + \frac{1}{\rho} \int_{z_b}^{z_s} \tau_{xx} dz \\ UVh + \frac{1}{\rho} \int_{z_b}^{z_s} \tau_{xy} dz \end{pmatrix}, \quad \mathbf{G} = \begin{pmatrix} Vh \\ VUh + \frac{1}{\rho} \int_{z_b}^{z_s} \tau_{xy} dz \\ V^2h + \frac{1}{\rho} \int_{z_b}^{z_s} \tau_{yy} dz \end{pmatrix}, \\
\mathbf{S} &= -\frac{1}{\rho} \begin{pmatrix} 0 \\ (\tau_{xx})_b \frac{\partial z_b}{\partial x} + (\tau_{xy})_b \frac{\partial z_b}{\partial y} - (\tau_{xz})_b \\ (\tau_{yy})_b \frac{\partial z_b}{\partial y} + (\tau_{xy})_b \frac{\partial z_b}{\partial x} - (\tau_{yz})_b \end{pmatrix}.
\end{aligned} \tag{2.34}$$

Equations (2.30) and (2.31) can also be transformed to a 2D vector notation (Peregrine 1967; Kim et al. 2009). To this end, let I be the auxiliary variable

$$I = \int_z^{z_s} w(x, y, z) dz', \tag{2.35}$$

and let the depth-averaged velocity vector \mathbf{U} be defined by

$$\mathbf{u} = \begin{pmatrix} U \\ V \end{pmatrix}. \tag{2.36}$$

The vertical velocity, as stated in Eq. (2.30), may then be rewritten as

$$w = -\nabla \cdot [\mathbf{u}(z - z_b)], \tag{2.37}$$

in which ∇ is the 2D Nabla operator defined by

$$\nabla = \left(\frac{\partial}{\partial x}, \frac{\partial}{\partial y} \right). \tag{2.38}$$

Inserting Eq. (2.37) into Eq. (2.35) leads, after integration, to

$$I = -\nabla \cdot \left[\mathbf{u} \frac{(h^2 - \eta^2)}{2} \right] + h[\mathbf{u} \cdot \nabla(h + z_b)]. \tag{2.39}$$

With this, Eq. (2.31) is rewritten as

$$\tau_{zz} = \rho g(h - \eta) + \rho \frac{\partial I}{\partial t} + \rho \nabla \cdot (I \mathbf{u}) - \rho w^2 + \int_z^{z_s} \left(\frac{\partial \tau_{zy}}{\partial y} + \frac{\partial \tau_{zx}}{\partial x} \right) dz'. \tag{2.40}$$

Equations (2.39) and (2.40) constitute the fundamental relations for modeling non-hydrostatic effects in depth-averaged models.

A scaling analysis reveals the importance of retaining w in vertically integrated models over steep terrain. Let $[x]$, $[y] = L$ and $[z] = H$ be horizontal and vertical scales in the Cartesian system of reference (x, y, z) . Similarly, also introducing the velocity scales $[u]$, $[v]$, $[w]$ for the horizontal ($[u]$, $[v]$) and vertical ($[w]$) velocity components, the space and velocity scale ratios are defined as

$$\frac{[w]}{[u]} = \frac{[w]}{[v]} = \varepsilon_{vel}, \quad \frac{[z]}{[x]} = \frac{[z]}{[y]} = \frac{H}{L} = \varepsilon_{spatial}. \quad (2.41)$$

Requesting the perseverance of the solenoidicity of the velocity field $[\text{div}(\mathbf{V}) = 0]$ by scaling then implies

$$\frac{[w]}{[u]} = \frac{[w]}{[v]} = \frac{H}{L} = \varepsilon, \quad \text{or} \quad \varepsilon_{spatial} = \varepsilon_{vel} = \varepsilon. \quad (2.42)$$

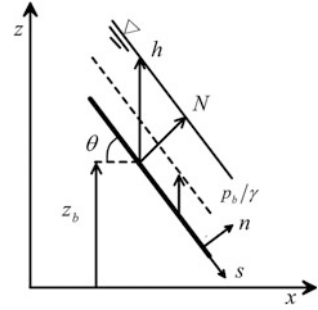
With the velocity scaling $[u] = (gL)^{1/2}$ and the time scaling $[t] = (L/g)^{1/2}$, one also readily deduces

$$\frac{[dw]}{[dt]} = \varepsilon(Lg)^{1/2}(g/L)^{1/2} = \varepsilon g. \quad (2.43)$$

For $\varepsilon \ll 1$, this result suggests that the vertical acceleration is asymptotically small as compared with g . Else, the hydrostatic pressure assumption is invalid and vertical accelerations must be accounted for. The above expressions for $[u]$ and $[t]$ automatically imply that gravity is important in the dimensionless mathematical description of the processes to be studied. Incidentally, the expressions for $[u]$ and $[t]$ differ from those of the shallow water equations (Friedrichs 1948); $[u]$ and $[t]$ would in those equations be scaled with H and not with L .

If the Cartesian coordinate system is now (s, n) , inclined by angle θ , then $[dw_n/dt] = g\varepsilon\cos\theta$, and with isotropic scaling ($\varepsilon = 1$) the bed normal acceleration w_n may be ignored for rapid gravity-driven flows on steep mountain slopes (as $\cos\theta$ is small). As an illustrative example, consider the simplest case of uniform flow down a steep slope (Fig. 2.3). In the curvilinear coordinates (s, n) following the terrain, the velocity is $U_s = q/N$, whereas the velocity in the n -direction is zero, with q as the discharge and N the flow thickness measured normal to the bed. Consider now the horizontal-vertical Cartesian coordinates (x, z) . The depth-averaged velocity in the x -direction reads $U_s = q/h$, with h as the vertical flow depth. From the bed kinematic boundary condition, the vertical velocity in the z -direction is $w = U\partial z_b/\partial x$.

Fig. 2.3 Uniform flow on a steep slope, highlighting differences between free surface flow depth h (gauge-measured, *solid line*), N (perpendicular to bottom), and (*dashed lines*) bottom pressure head p_b/γ (x) where $\gamma = \rho g$



The absolute velocity is then $V = (u^2 + w^2)^{1/2} = U(1 + \tan^2\theta)^{1/2}$. From Fig. 2.3, $N = h\cos\theta$, leading to $V = q/N$, which is identical to U_s . While in (s, n) coordinates, only U_s is non zero, u and w are of similar order of magnitude in horizontal-vertical Cartesian coordinates (x, z) . For example, on a steep slope of $\theta = 45^\circ$, $u = w = q/h$.

2.4 Simplified Forms of Non-hydrostatic Extended Flow Equations

2.4.1 RANS Model for River Flow

River flows are usually modeled using a depth-averaged model based on the Reynolds-Averaged Navier–Stokes (RANS) equations. Stresses are then made up of viscous and turbulent contributions. If the vertical velocity is neglected, then the flux vectors reduce to (Rodi 1980; Molls and Chaudhry 1995)

$$\mathbf{F} = \begin{pmatrix} U^2h + \frac{gh^2}{2} + \frac{1}{\rho}hT_{xx} \\ UVh + \frac{1}{\rho}hT_{xy} \end{pmatrix}, \quad \mathbf{G} = \begin{pmatrix} Vh \\ VUh + \frac{1}{\rho}hT_{xy} \\ V^2h + \frac{gh^2}{2} + \frac{1}{\rho}hT_{yy} \end{pmatrix}. \quad (2.44)$$

In these expressions, the hydrostatic pressure term has been substituted and the laminar viscous stress contributions are generally ignored. In that case, T_{xx} , T_{yy} , and T_{xy} are the depth-averaged turbulent stresses. These are determined by coupling an auxiliary turbulence system, e.g., the depth-averaged $k-\varepsilon$ model, or simply by using a constant eddy viscosity (Molls and Chaudhry 1995). If turbulent stresses are neglected, the system reduces to the classical 2D Saint-Venant equations (Liggett 1994; Vreugdenhil 1994).

2.4.2 One-Dimensional Water Waves Over Horizontal Topography

Consider the inviscid unsteady water wave propagation in a horizontal channel ($z_b = 0$) (Peregrine 1967, 1972), for which $\tau_{xx} = \tau_{zz} = p$ is the water pressure. Ignoring the last stress term on the RHS, Eq. (2.19) becomes

$$p(z) = \rho g(h - \eta) - \rho w^2 + \rho \frac{\partial}{\partial t} \int_z^{z_s} w dz' + \rho \frac{\partial}{\partial x} \int_z^{z_s} w u dz' + \rho \frac{\partial}{\partial y} \int_z^{z_s} w v dz'. \quad (2.45)$$

This is the general equation as developed by Nwogu (1993) for 2D water waves. Consider the depth-averaged approach for 1D flows, for which Eqs. (2.37) and (2.39) reduce to

$$w = -\eta \frac{\partial U}{\partial x}, \quad I = -\frac{\partial U}{\partial x} \frac{(h^2 - \eta^2)}{2}. \quad (2.46)$$

Inserting these expressions into Eq. (2.45) yields a parabolic pressure distribution p consisting of a hydrostatic term plus a quadratic dynamic correction including derivatives U_{xx} , U_x^2 , and U_{xt} as

$$\frac{p}{\rho} = g(h - \eta) + (U_x^2 - U_{xt} - UU_{xx}) \frac{(h^2 - \eta^2)}{2}. \quad (2.47)$$

Subscripts indicate, as above, partial differentiations with respect to the indicated variables. Equation (2.33) then simplifies to

$$\frac{\partial \mathbf{U}}{\partial t} + \frac{\partial \mathbf{F}}{\partial x} = \mathbf{0}, \quad \mathbf{U} = \begin{pmatrix} h \\ Uh \end{pmatrix}, \quad \mathbf{F} = \begin{pmatrix} Uh \\ M \end{pmatrix}, \quad M = U^2 h + \frac{1}{\rho} \int_{z_b}^{z_s} p dz. \quad (2.48)$$

In the free surface hydraulics literature (Montes 1998; Jain 2001), M is referred to as the momentum function, namely

$$M = \underbrace{g \frac{h^2}{2} + U^2 h}_{\text{Saint-Venant term}} + \underbrace{(U_x^2 - U_{xt} - UU_{xx}) \frac{h^3}{3}}_{\text{non-hydrostatic term}}. \quad (2.49)$$



Dennis Howell Peregrine was born on December 30, 1938, at Birkenhead, UK, and passed away at age 69 on March 29, 2007, at Bristol, UK. He joined the Mathematics Department of Bristol University in 1964, following his undergraduate and postgraduate training at Oxford and Cambridge Universities. He became member of a small but strong group of applied mathematicians in fluid dynamics then headed by Leslie Howarth (1911–2001). Up to his death, Peregrine played a key role in maintaining and promoting the study of fluids thereby ensuring that Bristol University remained one of the British centers of excellence in this discipline.

Peregrine's knowledge in the subject of water waves was encyclopedic. He concerned himself with their generation, propagation, and run-up, including their impact on coastal structures. His contributions are reflected in numerous publications among which his 1966 paper in the *Journal of Fluid Mechanics* (JFM) on the shallow water wave theory is particularly notable. More results that are recent include extremely high wave impact forces, including tsunami waves. The breaking of water waves is still under intense research, particularly as regards the energy dissipation process, the entrainment of air and sediment, and the generation of turbulence. Peregrine had a well-developed physical insight and skill in mathematical modeling. In addition, he served as associate editor of the JFM, where he processed an average of 50 research papers annually since 1981. He reached the retirement age in 2004 with little apparent change in his work-life balance. A successful event was held in 2005 in Bristol attracting colleagues from around the world to a lecture series in recognition of his contributions.

Thus, M gives rise to higher-order flow equations. The momentum function is composed of the leading order Saint-Venant (hydrostatic) term plus a Boussinesq (non-hydrostatic) correction. Equation (2.49) was originally derived by Serre (1953) and is extensively used in civil and environmental engineering applications (Basco 1983; Soares-Frazão and Zech 2002; Mohapatra and Chaudhry 2004; Chaudhry 2008). Equation (2.49) describes, e.g., the propagation of undular bores (Fig. 2.4), originally investigated by Peregrine (1966) using a finite difference model. Equations (2.48)–(2.49) are the so-called Serre (1953) equations for weakly dispersive, non-linear 1D water waves. The equations were later derived by Su and Gardner (1969) and Green and Naghdi (1976) using alternative theoretical methods. In coastal engineering, the equations are often named the *Serre-Green-Naghdi* equations. Using the irrotational flow theory, it can be demonstrated that the *Serre-*

Fig. 2.4 Undular bore propagating with breaking front (photograph by late Prof. D.H. Peregrine)



Green-Naghdi equations are regained if the variation of u with depth is accounted for (Su and Gardner 1969) (Chap. 3). Cienfuegos et al. (2006) presented finite volume numerical solutions of the extension of this system for variable bathymetry, whereas a detailed analytical investigation of the kinematic velocity field and the stability of solitary and cnoidal wave solutions of Eqs. (2.48)–(2.49) were given by Carter and Cienfuegos (2011). The first investigation of solitary and cnoidal wave solutions of the Serre equations was presented by Iwasa (1955, 1956), who independently derived the system of equations using the same depth-integrated approach of Serre (1953). For reviews of the *Serre-Green-Naghdi* equations and applications to coastal engineering, see Barthelemy (2004), Lannes and Bonneton (2009), Dias and Milewski (2010), and Bonneton et al. (2011).

2.4.3 Turbulent Uniform Flow on Steep Terrain

Consider turbulent water flow in the vertical plane (x, z) . Neglecting viscous contributions, the stress tensor is then $\tau_{xx} = p - \sigma_{xx}$, $\tau_{zz} = p - \sigma_{zz}$, and $\tau_{xz} = -\sigma_{xz}$, where σ denotes the turbulent Reynolds stress due to time averaging of the Navier–Stokes equations for fluid flow. The 2D vertically integrated x -momentum equation for turbulent water flows is, from Eq. (2.28),

$$\underbrace{\frac{\partial}{\partial t}(Uh) + \frac{\partial}{\partial x}(U^2h)} = -\frac{1}{\rho} \left[\underbrace{\frac{\partial}{\partial x} \int_{z_b}^{z_s} (p - \sigma_{xx}) dz}_{\text{bottom pressure}} + (p - \sigma_{xx})_b \frac{\partial z_b}{\partial x} + (\sigma_{xz})_b \right], \quad (2.50)$$

and from Eq. (2.20), the equation describing the bottom pressure is found to be

$$\underbrace{\frac{\partial}{\partial t}(\bar{w}h) + \frac{\partial}{\partial x}(\bar{w}Uh)} = \frac{1}{\rho} \left[(p - \sigma_{zz})_b + \underbrace{\frac{\partial}{\partial x} \int_{z_b}^{z_s} \sigma_{xz} dz}_{\text{}} + (\sigma_{xz})_b \frac{\partial z_b}{\partial x} \right] - gh. \quad (2.51)$$

Here, the depth-averaged vertical velocity is defined as

$$\bar{w}(x, y, t) = \frac{1}{h} \int_{z_b}^{z_s} w dz. \quad (2.52)$$

Uniform flow is typically defined in hydraulic engineering prescribing a constant flow depth for which the bed shear is in equilibrium with the gravity term of the momentum balance (Chow 1959). However, this definition is not rigorous; here, uniform flow on a slope is defined from a fluid mechanics perspective as an ideal state where the depth is constant and the distributions of velocity, pressure, and Reynolds stresses remain unchanged for any vertical section. Therefore, for uniform flow on a steep slope (Fig. 2.3) the underbraced terms in Eqs. (2.50) and (2.51) are zero by definition, and Eq. (2.50) reduces to the x -force (momentum) balance

$$(p - \sigma_{xx})_b \frac{\partial z_b}{\partial x} + (\sigma_{xz})_b = 0, \quad (2.53)$$

whilst the z -momentum balance, Eq. (2.51), collapses to the force balance

$$(p - \sigma_{zz})_b + (\sigma_{xz})_b \frac{\partial z_b}{\partial x} = \rho gh. \quad (2.54)$$

Consider an infinitesimal element at a basal point, subjected to plane strain, once referred to the (x, z) -axes and once inclined by the slope angle θ as shown in Fig. 2.5. The stress states in the (x, z) -coordinates and (s, n) -coordinates are then related to one another based on the equilibrium conditions of triangular elements by the equation (Fig. 2.5)

$$\begin{pmatrix} \sigma_{nn} \\ \sigma_{ss} \\ \tau_{sn} \end{pmatrix} = \begin{pmatrix} \cos^2 \theta & \sin^2 \theta & 2 \cos \theta \sin \theta \\ \sin^2 \theta & \cos^2 \theta & -2 \cos \theta \sin \theta \\ -\sin \theta \cos \theta & \sin \theta \cos \theta & \cos^2 \theta - \sin^2 \theta \end{pmatrix} \begin{pmatrix} \sigma_{xx} \\ \sigma_{zz} \\ \tau_{xz} \end{pmatrix}. \quad (2.55)$$

Simple shear along the bed slope is described by vanishing normal stresses $\sigma_{nn} = \sigma_{ss} = 0$ and $\tau_{sn} = \tau_b$. For this choice, the above system of equations is easily inverted with the solution given by

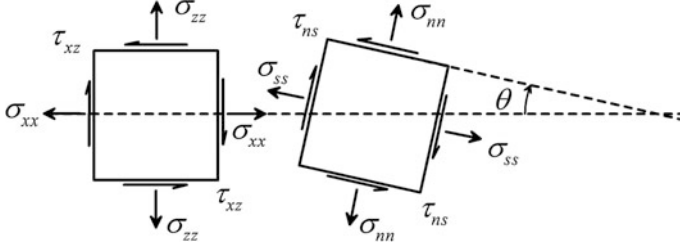


Fig. 2.5 Infinitesimal element subjected to plane stress referred to (x, z) - and (s, n) -coordinates rotated by angle θ

$$\begin{aligned}
 (\sigma_{zz})_b &= 2\tau_b \cos\theta \sin\theta, \\
 (\sigma_{xx})_b &= -2\tau_b \cos\theta \sin\theta, \\
 (\sigma_{xz})_b &= \tau_b (\cos^2\theta - \sin^2\theta).
 \end{aligned} \tag{2.56}$$

Here, τ_b is the shear stress in the s -direction, measured along the sloping plane (Fig. 2.3), and θ is given by $\partial z_b / \partial x = \tan\theta$. Inserting Eq. (2.56) into Eqs. (2.53) and (2.54) yields, respectively,

$$\tau_b = -p_b \tan\theta, \tag{2.57}$$

$$p_b = \rho g h + \tau_b \tan\theta. \tag{2.58}$$

Combining Eqs. (2.57) and (2.58) results in the non-hydrostatic bottom pressure on a steep slope as

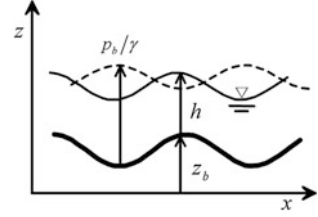
$$\frac{p_b}{\rho g} = \frac{h}{1 + \tan^2\theta} = h \cos^2\theta. \tag{2.59}$$

Equation (2.59) indicates that the bottom pressure on a steep slope is non-hydrostatic, which becomes important already for $\theta = 45^\circ$, as in this case a reduction in the bottom pressure of 50 % over the vertical water weight ensues. Equation (2.59) is a classical result obtained in the channel flow literature using gradually varied flow computations in the (s, n) system as shown in Fig. 2.3. Noting that $N = h \cos\theta$, Eq. (2.59) may be written as (e.g., Chow 1959; Henderson 1966)

$$\frac{p_b}{\rho g} = N \cos\theta. \tag{2.60}$$

Equation (2.60) is a particular non-hydrostatic result of the general formulation given by Eq. (2.51), where conditions of gradually varied flows are not assumed. This development demonstrates that non-hydrostatic pressures originate from the turbulent Reynolds stresses and not from the vertical velocity \bar{w} , given the fact that the gradient $\partial \bar{w} / \partial x$ is zero.

Fig. 2.6 Flow over undular bed $z_b(x)$ with (thin lines) free surface profile $h(x)$ and (dashed lines) bottom pressure head profile $p_b/\gamma(x)$



2.4.4 Flows Over Curved Beds

Flows over variable topography imply that the source term in Eq. (2.34) is not zero, i.e., resistive forces and bed geometrical source terms must be accounted for. In the geophysical environment, the effect of variable topography on the flow solution of dynamical models by stating conservation of mass and momentum is important. Such problems include atmospheric air currents over variable terrain (Sivakumaran and Dressler 1989) or water flows over fluvial bed forms, such as dunes and anti-dunes (Engelund and Hansen 1966; Dey 2014). Models for 1D flows over curved beds were proposed by Dressler (1978), Hager and Hutter (1984a, b), and Khan and Steffler (1996a, b). For steady 1D flows over a curved bed in the vertical plane given by $z_b = z_b(x)$ (Fig. 2.6), Eq. (2.28) reduces to

$$\frac{\partial}{\partial x}(hU^2) = -\frac{1}{\rho} \left[\frac{\partial}{\partial x} \int_{z_b}^{z_s} \tau_{xx} dz + (\tau_{xx})_b \frac{\partial z_b}{\partial x} - (\tau_{xz})_b \right]. \quad (2.61)$$

For frictionless fluids, the stress tensor is the pressure tensor for inviscid flow with $\tau_{xx} = p$ and $\tau_{xz} = 0$. Therefore, Eq. (2.61) can be further simplified to the ODE

$$\frac{dM}{dx} = -\frac{p_b}{\rho} \frac{\partial z_b}{\partial x}, \quad (2.62)$$

where

$$M = hU^2 + \int_{z_b}^{z_s} \frac{p}{\rho} dz. \quad (2.63)$$

Here, p_b is the basal pressure, and the free surface pressure has been set to zero. The vertical velocity for steady 1D flows over curved terrain is obtained from Eq. (2.37), using $q = \text{const} = U(x)h(x)$,

$$\begin{aligned}
w &= -\frac{\partial}{\partial x} [U(z - z_b)] = -\frac{\partial}{\partial x} \left[\frac{q}{h} (z - z_b) \right] = -\frac{\partial}{\partial x} \left[-\frac{q}{h^2} \frac{\partial h}{\partial x} (z - z_b) - \frac{q}{h} \frac{\partial z_b}{\partial x} \right] \\
&= U \left[\frac{\partial z_b}{\partial x} + \frac{\partial h}{\partial x} \frac{(z - z_b)}{h} \right].
\end{aligned} \tag{2.64}$$

Similarly, an expression for the pressure results from Eq. (2.40) as

$$\begin{aligned}
p = \tau_{zz} &= \rho g(z_s - z) + \rho \frac{\partial I}{\partial t} + \rho \frac{\partial}{\partial x} (IU) - \rho w^2 + \int_z^{z_s} \frac{\partial \tau_{zx}}{\partial x} dz' \\
&= \rho g(z_s - z) + \underbrace{\rho \frac{\partial}{\partial t} \left\{ \int_z^{z_s} w dz' \right\}}_{=0 \text{ (steady-state)}} + \rho \frac{\partial}{\partial x} \left\{ U \int_z^{z_s} w dz' \right\} - \rho w^2 + \underbrace{\int_z^{z_s} \frac{\partial \tau_{zx}}{\partial x} dz'}_{\text{neglected}},
\end{aligned} \tag{2.65}$$

or

$$p(z) = \rho g(z_s - z) - \rho w^2 + \rho \frac{\partial}{\partial x} \left(U \int_z^{z_s} w dz' \right). \tag{2.66}$$

In the above derivation, Eq. (2.40) has been employed in the spatially 1D version and under steady-state conditions. Moreover, the integrated shear stress flux term has been neglected as is common in the pertinent hydraulic literature. Inserting Eq. (2.64) into Eq. (2.66) and performing the relevant integration and differentiations yields

$$\frac{p(z)}{\rho g} = h - \eta + \frac{U^2}{2g} \left[2hz_{bxx} \left(1 - \frac{\eta}{h} \right) + (hh_{xx} - h_x^2) \left(1 - \frac{\eta^2}{h^2} \right) - 2h_x z_{bx} \left(1 - \frac{\eta}{h} \right) \right]. \tag{2.67}$$

Upon substitution into Eq. (2.63) and performing an additional integration, one obtains

$$M = g \frac{h^2}{2} + hU^2 \left(1 + \frac{hh_{xx} - h_x^2}{3} + \frac{hz_{bxx}}{2} - \frac{h_x z_{bx}}{2} \right). \tag{2.68}$$

The analysis to obtain these results is somewhat cumbersome, even though it is not difficult; it is, therefore, deferred to Appendix A.

The bottom pressure, from Eq. (2.67), is of the form

$$\frac{p_b}{\rho g} = h + \frac{U^2}{2g} [2hz_{bxx} + hh_{xx} - h_x^2 - 2h_x z_{bx}]. \quad (2.69)$$

Equation (2.69) was first derived by Castro-Orgaz and Hager (2009) and solved using a Picard iteration solution of the irrotational flow equations, as described in Chap. 3; it highlights a key ingredient of the Boussinesq theory: Differences between the flow depth h and the bottom pressure head p_b/γ are adequately accounted for. In general, at locations with positive flow curvature (concave bed), one has $p_b/\gamma > h$, whereas $p_b/\gamma < h$ at locations with negative flow curvature (convex bed), see Fig. 2.6. If the same flow is computed using a pure Saint-Venant theory, the free surface is not accurately predicted, because the vertical acceleration is not accounted for, while the bottom pressure can simply not be predicted, given that $p_b/\gamma = h$ is assumed ab initio. This is a strong reason to adopt the Boussinesq theory in geophysical, environmental, civil, and coastal research, given that the increase in computational effort is moderate, but the gain in physical appropriateness is high.

2.4.5 Enhanced Gravity

Denlinger and Iverson (2004) and Denlinger and O’Connell (2008) presented a simplified vertically integrated, unsteady non-hydrostatic model in which a key physical element was introduced. They defined a corrected (or “enhanced”) gravity acceleration, in which the effect of vertical acceleration is accounted for. Their equation of vertical pressure at the bed level in a turbulent water flow is

$$p_b = \rho gh + \rho \left(\frac{\partial(\bar{w}h)}{\partial t} + \frac{\partial(\bar{w}Uh)}{\partial x} + \frac{\partial(\bar{w}Vh)}{\partial y} \right) = \rho g' h. \quad (2.70)$$

In Eq. (2.70), g' is the enhanced gravity, including a mean vertical acceleration $D\bar{w}/Dt$ as

$$g' = g + \frac{D\bar{w}}{Dt} = g + \frac{\partial\bar{w}}{\partial t} + U \frac{\partial\bar{w}}{\partial x} + V \frac{\partial\bar{w}}{\partial y}. \quad (2.71)$$

As to the depth-averaged velocity, these authors used the mean value

$$\bar{w} = \frac{1}{2} (w_s + w_b), \quad (2.72)$$

in which w_s and w_b are determined from Eqs. (2.7) and (2.8), respectively. Equation (2.72) permits the evaluation of p_b from Eq. (2.70). Denlinger and Iverson (2004) further assumed that $p(z)$ is linearly distributed in z as

$$p(z) = \rho g'(h - \eta). \quad (2.73)$$

Steffler and Jin (1993), who also used Eq. (2.73) to produce Boussinesq-type behavior in hydraulic structures, further considered relations that are more complex. Using g' , the inclusion of non-hydrostatic effects on vertically integrated models becomes conceptually simple, allowing for their straightforward inclusion into Riemann solvers (Sect. 2.6).

Let us now compare the physical simplifications underlying the enhanced gravity concept with the general mathematical theory presented above. For this purpose, from the general Eq. (2.20) at the bed level, and by neglecting the stress integral, one deduces the equation

$$p_b = \rho gh + \rho \frac{\partial}{\partial t} \int_{z_b}^{z_s} w dz + \rho \frac{\partial}{\partial x} \int_{z_b}^{z_s} w u dz + \rho \frac{\partial}{\partial y} \int_{z_b}^{z_s} w v dz. \quad (2.74)$$

Using Eq. (2.72) for \bar{w} , Eq. (2.74) becomes identical to Eq. (2.70). Therefore, the bottom pressure p_b used by Denlinger and Iverson (2004) is an exact depth-averaged value. However, $p(z)$ as given by Eq. (2.73) is assumed to be linearly distributed, whereas a parabolic distribution results from Eq. (2.40) (see Appendix A). Denlinger and Iverson's (2004) approximation to the vertical pressure distribution introduces some error in the momentum computation, despite the exact bed value. The physical significance of the enhanced gravity correction is elucidated using steady 1D flow over curved terrain as a test case. In this case, Eq. (2.71) reduces under steady state to

$$g' = g + \frac{D\bar{w}}{Dt} = g + U \frac{\partial \bar{w}}{\partial x}. \quad (2.75)$$

From steady, spatially 1D versions of Eqs. (2.7), (2.8) and with Eq. (2.72), as well as for uniform velocity $u(z) = U$, one obtains

$$\bar{w} = \frac{1}{2}(w_s + w_b) = \frac{1}{2}[U(h_x + z_{bx}) + Uz_{bx}], \quad (2.76)$$

and after differentiation

$$\frac{\partial \bar{w}}{\partial x} = U_x \left(\frac{h_x}{2} + z_{bx} \right) + U \left(\frac{h_{xx}}{2} + z_{bxx} \right). \quad (2.77)$$

Inserting Eq. (2.77) into Eq. (2.75), using the expression $U_x = -(q/h^2)h_x$ and inserting the resulting g' into Eq. (2.70), yields the bed pressure of the Denlinger and Iverson (2004) theory for this flow problem as

$$p_b = \rho gh + \rho \frac{U^2}{2} (hh_{xx} - h_x^2 - 2h_x z_{bx} + 2hz_{bxx}). \quad (2.78)$$

This agrees with Eq. (2.69) for the generalized Boussinesq theory. It also corresponds to the bed pressure of Khan and Steffler's (1996a, b) Boussinesq model for 1D steady flow over a curved bed, if turbulent stresses and bed friction forces are neglected. Inserting the linear pressure of Eq. (2.73) into the expression for the flow momentum M , Eq. (2.63), results in

$$M = g \frac{h^2}{2} + hU^2 \left(1 + \frac{hh_{xx} - h_x^2}{4} + \frac{hz_{bxx}}{2} - \frac{h_x z_{bx}}{2} \right). \quad (2.79)$$

Comparing Eqs. (2.68) and (2.79), it is noted that the enhanced gravity approach introduces a factor (1/4) in the water-depth derivative-correction term as compared with (1/3) in the exact vertically integrated equations. Therefore, the corrected enhanced gravity in Serre's theory (1953) in a horizontal channel is given by

$$g' = g + \frac{4}{3} \frac{D\bar{w}}{Dt} = g + \frac{4}{3} U \frac{\partial \bar{w}}{\partial x}. \quad (2.80)$$

In turn, the flow momentum in the x -direction is, therefore, given by

$$M = U^2 h + g' \frac{h^2}{2} = g \frac{h^2}{2} + hU^2 \left(1 + \frac{hh_{xx} - h_x^2}{3} \right), \quad (2.81)$$

as shown by Serre (1953) and Benjamin and Lighthill (1954).

2.4.6 Non-hydrostatic Model Including Friction Effects

Steffler and Jin (1993) and Khan and Steffler (1996a, b) developed a Boussinesq-type momentum model, in which both acceleration and frictional effects were accounted for in generating non-hydrostatic pressure distributions over steep and curved beds. This model can be deduced from the generalized equations presented in this text. Neglecting depth-averaged turbulent stresses, the full Eqs. (2.50) and (2.51) take the forms

$$\frac{\partial}{\partial t}(Uh) + \frac{\partial}{\partial x} \left(U^2 h + \int_{z_b}^{z_s} \frac{p}{\rho} dz \right) = -\frac{1}{\rho} \left[(p - \sigma_{xx})_b \frac{\partial z_b}{\partial x} + (\sigma_{xz})_b \right], \quad (2.82)$$

$$\frac{\partial}{\partial t}(\bar{w}h) + \frac{\partial}{\partial x}(\bar{w}Uh) = \frac{1}{\rho} \left[(p - \sigma_{zz})_b + (\sigma_{xz})_b \frac{\partial z_b}{\partial x} \right] - gh. \quad (2.83)$$

Inserting Eq. (2.56) for a pure bed shear into Eqs. (2.82) and (2.83) gives

$$\frac{\partial}{\partial t}(Uh) + \frac{\partial}{\partial x} \left(U^2h + \int_{z_b}^{z_s} \frac{p}{\rho} dz \right) = -\frac{p_b}{\rho} \frac{\partial z_b}{\partial x} - \frac{\tau_b}{\rho}, \quad (2.84)$$

as well as

$$p_b = \rho gh + \rho \frac{\partial}{\partial t}(\bar{w}h) + \rho \frac{\partial}{\partial x}(\bar{w}Uh) + \tau_b \frac{\partial z_b}{\partial x}. \quad (2.85)$$

In Eq. (2.85) the depth-averaged vertical velocity \bar{w} is given by Eq. (2.72), with w_s and w_b computed from the kinematic boundary conditions, i.e., Eqs (2.7) and (2.8) (Steffler and Jin 1993). A distribution $p = p(z)$ must be introduced into Eq. (2.84) for model closure. A linear distribution was assumed, corresponding to the approximation of Denlinger and Iverson (2004). Equation (2.84) then reduces, after integration, to

$$\frac{\partial}{\partial t}(Uh) + \frac{\partial}{\partial x} \left(U^2h + \frac{hp_b}{2} \right) = -\frac{p_b}{\rho} \frac{\partial z_b}{\partial x} - \frac{\tau_b}{\rho}. \quad (2.86)$$

This equation is the Boussinesq-type x -momentum equation developed by Khan and Steffler (1996a, b). For steady flow, and after using Eq. (2.72) to eliminate \bar{w} from Eq. (2.85), Eqs. (2.84), and (2.85) reduce to

$$\frac{d}{dx} \left(U^2h + \frac{hp_b}{2} \right) = -\frac{p_b}{\rho} \frac{\partial z_b}{\partial x} - \frac{\tau_b}{\rho}, \quad (2.87)$$

$$p_b = \rho gh + \rho \frac{U^2}{2} (hh_{xx} - h_x^2 - 2h_x z_{bx} + 2hz_{bxx}) + \tau_b \frac{\partial z_b}{\partial x}. \quad (2.88)$$

From these equations, the flow momentum is

$$M = g \frac{h^2}{2} + hU^2 \left(1 + \frac{hh_{xx} - h_x^2}{4} + \frac{hz_{bxx}}{2} - \frac{h_x z_{bx}}{2} \right) + \frac{hz_{bx} \tau_b}{2\rho}. \quad (2.89)$$

A typical non-hydrostatic flow, in which friction effects need to be accounted for, is the undular hydraulic jump (Fawer 1937; Serre 1953; Montes 1986) as shown in Fig. 2.7. Note that upon comparing Eq. (2.89) with Eqs. (2.68) and (2.79), both the theories of Denlinger and Iverson (2004) and of Castro-Orgaz and Hager (2009) do not account for the bed-shear resistance. This is also noted upon comparing Eq. (2.88) with Eqs. (2.69) and (2.78) for the bottom pressure p_b .



Fig. 2.7 Undular hydraulic jump. Note the highly 3D free surface flow pattern (photograph VAW, ETH Zurich)

The present development, however, allows for inclusion of basal (but not interior) frictional effects in Boussinesq-type computations if large computational domains are considered.

2.5 Sediment Transport and Movable Beds

2.5.1 Introduction

Most of the dynamic models for bed-form evolution are based on the sediment mass conservation equation, also referred to as the Exner equation. It reads (Chaudhry 2008)

$$(1 - n) \frac{\partial z_b}{\partial t} = - \frac{\partial q_b}{\partial x}, \quad (2.90)$$

with n as the bed porosity, z_b bed elevation (interface of bed-load layer with clear-water flow), t time, and x longitudinal coordinate. The Saint-Venant equations stating the depth-integrated mass and momentum balances of the water flow are, with the water discharge q and the friction slope S_f ,

$$\frac{\partial q}{\partial x} + \frac{\partial h}{\partial t} = 0, \quad \frac{1}{g} \frac{\partial q}{\partial t} + \frac{\partial}{\partial x} \left(\frac{q^2}{gh} + \frac{h^2}{2} \right) = h \left(- \frac{\partial z_b}{\partial x} - S_f \right). \quad (2.91)$$

In this system, the dominant mode of sediment transport is assumed to be bed load, neglecting, e.g., the suspended (so-called wash) load transport. According to Yalin (1977), the unit bed-load transport rate q_b is written in dimensionless form as

$$q_b^* = f \left(\tau^*, R, R_{ep}, S_o, \frac{h}{D} \right). \quad (2.92)$$

For the derivation of such formulas, see Hutter and Wang (2016). In Eq. (2.92), $q_b^* = q_b/(RgD^3)^{1/2}$ and $\tau^* = \tau_b/(\gamma RD)$ are dimensionless discharge and basal shear stress variables, g is the gravity acceleration, τ_b the bottom shear stress, $R = (\gamma_s/\gamma) - 1$ the submerged specific gravity, or ratio between the fluid, γ , and sediment-specific weights γ_s ; D is a representative particle diameter, $Re_p = (RgD)^{1/2}D/\nu$ the particle Reynolds number, that depends on the kinematic viscosity ν , S_o the bed slope, and h the water depth.

Equation (2.92) was principally developed at two institutions to obtain a simplified practical form allowing for a mechanistic interpretation. The *first* school followed the work of Einstein (1950), who considered a bed-load layer disconnected from the upper layer where finer sediment particles were entrained by fluid turbulence. The movement of the solid particles in jumps, or by saltations, was based on its stochastic formulation. The final expression contained coefficients that were fitted to the available experimental data. Einstein considered the saltation of particles as a mode of suspended sediment transport.

The *second* school followed the work of Bagnold (1973), who proposed an alternative method where the bed-load rate is related to the motive power of the moving fluid, i.e., the product of shear stress and fluid velocity, weighted with an efficiency coefficient. Both Einstein and Bagnold's expressions have a theoretical foundation, yet empirical coefficients are used to fit the experimental data. As Garcia (2008) indicated in his review, the current scientific community tends away from Einstein's formulation toward Bagnold's description of bed-load transport. Following the empirical proposals of the early formulas, his model includes a critical or threshold value of the shear stress, τ_c , normalized as τ_c^* , for the inception of the sediment motion, based on the formulation of Shields (Buffington and Montgomery 1997). Using this concept, and assuming uniform flow over gentle slope (S_o in Eq. 2.92 is neglected), Eq. (2.92) simplifies in this case to

$$q_b^* = f(\tau^*, \tau_c^*, \text{fitting parameters}). \quad (2.93)$$

The main physical insight extracted from this framework is that sediment is entrained by a fluid flow once a critical value of the shear stress is reached. This implies that the moving grains extract momentum from the fluid within the bed-load layer to keep the shear stress at the critical value for motion. This type of bed-load formulation has been widely used to obtain fits in both laboratory and field conditions (Schmocker 2011), and constitutes the basis of open-channel flow models, incorporating sediment transport and movable bed features (Chaudhry 2008). One empirical relation based on Eq. (2.93) of wide acceptance is the expression of Meyer-Peter and Müller (1948). Other mechanistic treatments added more insight to the process of bed-load transport including the saltation model of Wiberg and Smith (1989) or the stochastic model of sediment dynamics of Ancy (2010) and Furbish et al. (2012). However, Eq. (2.93) predominates in open-channel flow models. Table 2.1 shows common expressions of Eq. (2.93).

The Saint-Venant model is based on hydrostatic pressure distributions, so that it is limited to gradually varied flows with almost parallel streamlines. A corollary is

Table 2.1 Dimensionless bed-load transport equations for q_b^* , with variables of Eqs. (2.92) and (2.93), f as fitting coefficient and U^* as dimensionless average particle horizontal velocity

Author(s)	q_b^*
Meyer-Peter and Müller (1948)	$8(\tau^* - \tau_c^*)^{3/2}$
Einstein (1950)	$12f(\tau^* - \tau_c^*)^{3/2}$
Bagnold (1973)	$U^*(\tau^* - \tau_c^*)$
Engelund and Fredsoe (1976)	$18.74(\tau^* - \tau_c^*)(\sqrt{\tau^*} - 0.7\sqrt{\tau_c^*})$
Parker (1979)	$11.2(\tau^* - \tau_c^*)^{4.5}\tau_c^{*-3}$

that the application of Eqs. (2.91) and (2.93) requires planar beds, lower-regime flow conditions, i.e., bed forms due to the erosion and deposition processes are not accounted for. However, despite these limitations, the equations listed in Table 2.1 are commonly coupled with Eqs. (2.91)–(2.93) in morphodynamic open-channel flow models (Garcia 2008) with the purpose of predicting the temporal and spatial evolutions of the four variables $q(x, t)$, $h(x, t)$, $q_b(x, t)$, and $z_b(x, t)$. These applications should therefore be restricted to weakly erodible beds under uniform or gradually varied water flows. The models are therefore defined as gradually varied geomorphodynamic models. Despite efforts over the past half century, the prediction of flows and sediment transports over bed forms still presents a major challenge for the solution of sedimentation problems (ASCE 2002). The basic question still needed to be addressed for sediment transport is: “What are the expected flow depths and sediment transport rates for given sediment and fluid characteristics, channel geometry, and discharge?” The answer remains highly uncertain, and much of the uncertainty can be traced to the development of bed forms (ASCE 2002). This source explains that several hydraulic laboratories are currently devoting appreciable experimental efforts to explore, at very small scale, the details of bed-load transport (Ancey 2010; Lajeunesse et al. 2010). Given the limitations stated for the gradually varied geomorphodynamic model, the complex cases of the evolution of bed forms for streams, where both the streamline curvature and bottom slope may affect the bed load, need advanced theoretical approaches.

Figure 2.8 shows some typical bed forms in natural streams, adapted from Engelund and Fredsoe (1982). The undular flow over the bed form may be entirely subcritical (Fig. 2.8a), supercritical (Fig. 2.8b), or involve transcritical flow changing from sub- to supercritical conditions, and vice versa (Fig. 2.8c), forming an undular hydraulic jump (Chanson 2000; Castro-Orgaz and Hager 2011c). Dunes correspond to asymmetrical sand waves appearing beneath subcritical water flows, roughly out of phase with the bed shape. Antidunes are wave-like bed forms appearing beneath a supercritical stream and practically in-phase with the bed geometry. Undular hydraulic jumps are an intermediate configuration where both flow features occur. The sediment motion is induced by the water wave action at wave troughs and crests of the undular flow, respectively, revealing distinctive 3D flow features where friction and inertial forces are predominant.

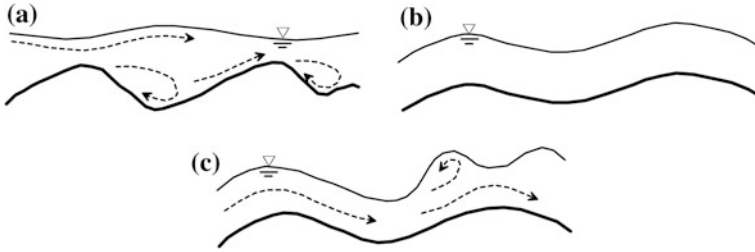


Fig. 2.8 Bed forms **a** dune, **b** antidune, **c** transcritical profile from super- to subcritical flows with undular hydraulic jump and wave breaking (adapted from Engelund and Fredsoe 1982)

The flow over curved bed forms, such as dunes or antidunes, plays a major role in the establishment of flow resistance (Kennedy 1963; Engelund and Hansen 1966; Graf and Altinakar 1996). The curvature on water flows, provoked by the bed forms, causes vertical accelerations of water particles, inducing a non-hydrostatic pressure distribution (Engelund and Hansen 1966; Bose and Dey 2009). Therefore, the gradually varied morphodynamic model described above is inappropriate to study flow over curved bed forms. Figure 2.9 shows water flow over a dune. The streamlines adjust to the shape of the sand wave, and undulations develop at the water surface. Turbulent drag over the sand wave provokes intense erosion at the downstream dune side, and a free streamline separates from the bed sediment surface, trapping a vortex flow zone below. The water surface profile $h = h(x)$ over the curved bed is a function of the local values of dh/dx , d^2h/dx^2 , dz_b/dx , and d^2z_b/dx^2 (Engelund and Hansen 1966; Hager and Hutter 1984a, Bose and Dey 2009; Castro-Orgaz et al. 2015), where $z_b = z_b(x)$ is the longitudinal profile of the bed form. The extended momentum conservation equation for water flow above a sand wave is approximated by a steady-state equation of the form (Engelund and Hansen 1966; Onda and Hosoda 2004)

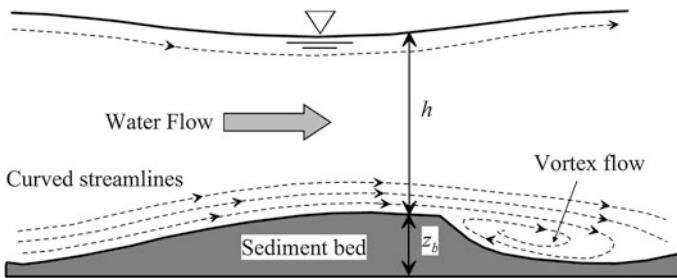


Fig. 2.9 Water flow across a dune with streamline pattern including recirculating flow

$$\begin{aligned} \frac{dM}{dx} &= -\frac{p_b}{\rho} \frac{dz_b}{dx} - \frac{\tau_b}{\rho}, \\ M &= \frac{h^2}{2} + U^2 h \left(1 + \frac{1}{3} h \frac{d^2 h}{dx^2} - \frac{1}{3} \left(\frac{dh}{dx} \right)^2 + \frac{1}{2} h \frac{d^2 z_b}{dx^2} - \frac{1}{2} \frac{dh}{dx} \frac{dz_b}{dx} \right). \end{aligned} \quad (2.94)$$

Here, M is the specific momentum and p_b the actual (non-hydrostatic) pressure at the curved sediment bed surface. The solution of the system, given by Eq. (2.94) for a given water discharge, bed-form profile, and appropriate boundary conditions produces the local free surface profile $h = h(x)$. The bed profile is updated based on Exner's Eq. (2.90) for the next time cycle. Onda and Hosoda (2004) also parametrized the bed-shear stress using the near-bed velocity and corrected the local skin friction coefficient with a free surface and sediment-bed slope factor. The bed-form profile $z_b(x)$ -configuration will affect the profile $h = h(x)$ of the free surface that, in turn, affects the bed-shear stress and then the bed-load transport rate under non-uniform flow conditions, involving curvilinear streamlines and non-hydrostatic pressures. Therefore, non-hydrostatic models are more suitable to account for bed-form processes. At the downstream dune face, erosion results in a vortex-flow zone with recirculation, for which non-hydrostatic 1D models do not account for, unless the momentum of the recirculating bubble is accounted for by a simplified flow model, or an empirical estimator, into the streamwise momentum balance.

2.5.2 *Non-hydrostatic Unsteady Free Surface Flow with Bed-Load Sediment Transport*

Sediment transport problems, such as bed-form migration, involve a vertical length scale of the order of the horizontal length scale, leading to non-hydrostatic flow conditions as pointed out previously. In this section, the non-hydrostatic unsteady sediment transport model over erodible beds is developed by accounting for bed-load motion. The development is shown to be a generalization of the theory by Engelund and Hansen (1966) for flow in alluvial streams. Neglecting depth-averaged turbulent stresses, Eq. (2.50) reduces to

$$\frac{\partial}{\partial t}(Uh) + \frac{\partial}{\partial x}(U^2 h) = -\frac{1}{\rho} \left[\frac{\partial}{\partial x} \int_{z_b}^{z_s} p dz + (p - \sigma_{xx})_b \frac{\partial z_b}{\partial x} + (\sigma_{xz})_b \right]. \quad (2.95)$$

Using Eq. (2.56) for a pure bed-shear state one finds

$$-(\sigma_{xx})_b \frac{\partial z_b}{\partial x} + (\sigma_{xz})_b = -\tau_b. \quad (2.96)$$

Assuming a linear pressure distribution

$$p = p_b \left(1 - \frac{\eta}{h}\right) = (p_1 + \rho gh) \left(1 - \frac{\eta}{h}\right), \quad (2.97)$$

where p_1 is the difference between the actual p_b and the hydrostatic bottom pressure (ρgh), the pressure force is

$$\int_{z_b}^{z_s} p dz = \int_0^h p d\eta = \rho g \frac{h^2}{2} + \frac{hp_1}{2}. \quad (2.98)$$

Inserting Eqs. (2.96) and (2.98) into Eq. (2.95) results in

$$\frac{\partial}{\partial t}(Uh) + \frac{\partial}{\partial x} \left(U^2 h + g \frac{h^2}{2} + \frac{hp_1}{2\rho} \right) = -\frac{p_b}{\rho} \frac{\partial z_b}{\partial x} - \frac{\tau_b}{\rho}. \quad (2.99)$$

The relation describing bottom pressure is Eq. (2.51); neglecting turbulent stresses, it is simplified to

$$\frac{p_b}{\rho} = gh + \frac{\partial}{\partial t}(\bar{w}h) + \frac{\partial}{\partial x}(\bar{w}Uh), \quad (2.100)$$

with the depth-averaged vertical velocity given by

$$\bar{w} = \frac{w_s + w_b}{2}. \quad (2.101)$$

Moreover, the free surface and bed kinematic boundary conditions are, respectively,

$$w_s = \frac{\partial}{\partial t}(h + z_b) + U \frac{\partial}{\partial x}(h + z_b), \quad (2.102)$$

$$w_b = \frac{\partial z_b}{\partial t} + U \frac{\partial z_b}{\partial x}. \quad (2.103)$$

Here, the bed level z_b is the interface of the bed-load layer with the clear-water flow. With the mean vertical acceleration given by

$$\frac{D\bar{w}}{Dt} = \frac{\partial \bar{w}}{\partial t} + U \frac{\partial \bar{w}}{\partial x}, \quad (2.104)$$

Equations (2.99) and (2.100) are rewritten as

$$\frac{\partial}{\partial t}(Uh) + \frac{\partial}{\partial x} \left(U^2 h + g \frac{h^2}{2} + \frac{D\bar{w}}{Dt} \frac{h^2}{2} \right) = -\frac{p_b}{\rho} \frac{\partial z_b}{\partial x} - \frac{\tau_b}{\rho}, \quad (2.105)$$

$$\frac{p_b}{\rho} = gh + \frac{p_1}{\rho} = gh + h \frac{D\bar{w}}{Dt}. \quad (2.106)$$

Note from Eq. (2.106) that the Boussinesq-type theories of Khan and Steffler (1996a) and Denlinger and Iverson (2004) are structurally identical. To find a closed form model, the boundary conditions, Eqs. (2.102) and (2.103), are inserted into Eq. (2.101), so that

$$\bar{w} = \frac{1}{2} \left(\frac{\partial h}{\partial t} + U \frac{\partial h}{\partial x} \right) + \frac{\partial z_b}{\partial t} + U \frac{\partial z_b}{\partial x}. \quad (2.107)$$

Using the depth-averaged continuity equation

$$\frac{\partial h}{\partial t} + \frac{\partial}{\partial x}(Uh) = 0 \quad \Rightarrow \quad \frac{\partial h}{\partial t} = -U \frac{\partial h}{\partial x} - h \frac{\partial U}{\partial x}. \quad (2.108)$$

With w_b as the bed contribution, accounting for the spatial and temporal variations of the sediment bed profile $z_b = z_b(x, t)$, Eq. (2.107) reduces to

$$\bar{w} = -\frac{h}{2} \frac{\partial U}{\partial x} + w_b, \quad w_b = \frac{\partial z_b}{\partial t} + U \frac{\partial z_b}{\partial x}. \quad (2.109)$$

Using Eqs. (2.109), Eq. (2.104) is rewritten as

$$\frac{D\bar{w}}{Dt} = (U_x^2 - U_{xt} - UU_{xx}) \frac{h}{2} + \frac{Dw_b}{Dt}, \quad (2.110)$$

in which the material derivative of w_b is defined as

$$\frac{Dw_b}{Dt} = \frac{\partial w_b}{\partial t} + U \frac{\partial w_b}{\partial x}. \quad (2.111)$$

The flow momentum M , defined by

$$M = U^2 h + \int_{z_b}^{z_s} \frac{p(z)}{\rho} dz, \quad (2.112)$$

is evaluated by using the linear pressure profile

$$p = p_b \left(1 - \frac{\eta}{h}\right). \quad (2.113)$$

It satisfies the vanishing free surface pressure condition and the basal pressure assignment $p(z_b) = p_b$. Substituting Eq. (2.106) yields

$$p = \left(\rho g + \rho \frac{D\bar{w}}{Dt}\right)(h - \eta). \quad (2.114)$$

The integral of this pressure distribution is

$$\int_{z_b}^{z_s} p dz = \int_0^h p d\eta = \rho \left(g + \frac{D\bar{w}}{Dt}\right) \frac{h^2}{2}, \quad (2.115)$$

which leads to

$$M = U^2 h + \int_{z_b}^{z_s} \frac{p(z)}{\rho} dz = U^2 h + \left(g + \frac{D\bar{w}}{Dt}\right) \frac{h^2}{2}. \quad (2.116)$$

When substituting Eq. (2.110), this yields

$$M = U^2 h + \int_{z_b}^{z_s} \frac{p(z)}{\rho} dz = U^2 h + g \frac{h^2}{2} + (U_x^2 - U_{xt} - UU_{xx}) \frac{h^3}{4} + \frac{h^2}{2} \frac{Dw_b}{Dt}. \quad (2.117)$$

The total time derivative Dw_b/Dt is determined by using Eqs. (2.109)₂ and (2.111), namely

$$\frac{\partial w_b}{\partial t} = \frac{\partial^2 z_b}{\partial t^2} + \frac{\partial U}{\partial t} \frac{\partial z_b}{\partial x} + U \frac{\partial^2 z_b}{\partial x \partial t}, \quad (2.118)$$

$$\frac{\partial w_b}{\partial x} = \frac{\partial^2 z_b}{\partial x \partial t} + \frac{\partial U}{\partial x} \frac{\partial z_b}{\partial x} + U \frac{\partial^2 z_b}{\partial x^2}, \quad (2.119)$$

so that

$$\begin{aligned} \frac{Dw_b}{Dt} = & \underbrace{\frac{\partial^2 z_b}{\partial t^2}}_{\frac{\partial}{\partial t} \left(-\frac{1}{1-n} \frac{\partial q_b}{\partial x} \right)} + \frac{\partial U}{\partial t} \frac{\partial z_b}{\partial x} + \underbrace{\left(U \frac{\partial^2 z_b}{\partial x \partial t} + U \frac{\partial^2 z_b}{\partial x \partial t} \right)}_{2U \frac{\partial^2 z_b}{\partial x \partial t} = 2U \frac{\partial}{\partial x} \left(-\frac{1}{1-n} \frac{\partial q_b}{\partial x} \right)} + \left[U \left(\frac{\partial U}{\partial x} \frac{\partial z_b}{\partial x} + U \frac{\partial^2 z_b}{\partial x^2} \right) \right]. \end{aligned} \quad (2.120)$$

Here, the Exner equation has been used as indicated in the sub-braced terms. For time and space independent porosity, this reduces to

$$\frac{Dw_b}{Dt} = -\frac{1}{(1-n)} \frac{\partial^2 q_b}{\partial x \partial t} - \frac{2U}{(1-n)} \frac{\partial^2 q_b}{\partial x^2} + \frac{\partial U}{\partial t} \frac{\partial z_b}{\partial x} + U \frac{\partial U}{\partial x} \frac{\partial z_b}{\partial x} + U^2 \frac{\partial^2 z_b}{\partial x^2}. \quad (2.121)$$

An alternative expression for M is, thus, given by

$$M = U^2 h + g \frac{h^2}{2} + (U_x^2 - U_{xt} - UU_{xx}) \frac{h^3}{4} + \left(-\frac{1}{(1-n)} \frac{\partial^2 q_b}{\partial x \partial t} - \frac{2U}{(1-n)} \frac{\partial^2 q_b}{\partial x^2} + \frac{\partial U}{\partial t} \frac{\partial z_b}{\partial x} + U \frac{\partial U}{\partial x} \frac{\partial z_b}{\partial x} + U^2 \frac{\partial^2 z_b}{\partial x^2} \right) \frac{h^2}{2}. \quad (2.122)$$

The corresponding bed pressure, Eq. (2.106), is then determined by

$$\begin{aligned} \frac{p_b}{\rho} &= gh + h \frac{D\bar{w}}{Dt} \\ &= gh + h \left[(U_x^2 - U_{xt} - UU_{xx}) \frac{h}{2} - \frac{1}{(1-n)} \frac{\partial^2 q_b}{\partial x \partial t} - \frac{2U}{(1-n)} \frac{\partial^2 q_b}{\partial x^2} \right. \\ &\quad \left. + \frac{\partial U}{\partial t} \frac{\partial z_b}{\partial x} + U \frac{\partial U}{\partial x} \frac{\partial z_b}{\partial x} + U^2 \frac{\partial^2 z_b}{\partial x^2} \right]. \end{aligned} \quad (2.123)$$

This equation holds only for $n = \text{const.}$ Moreover, for vanishing bed transport ($q_b = 0$), the bed is not eroded and, thus, does not evolve in time [$z_b = z_b(x)$]. The resulting flow momentum is then obtained as

$$M = U^2 h + g \frac{h^2}{2} + (U_x^2 - U_{xt} - UU_{xx}) \frac{h^3}{4} + \left(\frac{\partial U}{\partial t} \frac{\partial z_b}{\partial x} + U \frac{\partial U}{\partial x} \frac{\partial z_b}{\partial x} + U^2 \frac{\partial^2 z_b}{\partial x^2} \right) \frac{h^2}{2}. \quad (2.124)$$

If unsteady flow terms are neglected,

$$M = U^2 h + g \frac{h^2}{2} + (U_x^2 - UU_{xx}) \frac{h^3}{4} + \left(U \frac{\partial U}{\partial x} \frac{\partial z_b}{\partial x} + U^2 \frac{\partial^2 z_b}{\partial x^2} \right) \frac{h^2}{2}, \quad (2.125)$$

or

$$M = g \frac{h^2}{2} + U^2 h \left(1 + \frac{h}{4} \frac{d^2 h}{dx^2} - \frac{1}{4} \left(\frac{dh}{dx} \right)^2 + \frac{1}{2} h \frac{d^2 z_b}{dx^2} - \frac{1}{2} \frac{dh}{dx} \frac{dz_b}{dx} \right). \quad (2.126)$$

Retaining only curvature terms, one finally arrives at the basic equation used by Engelund and Hansen (1966)

$$M = g \frac{h^2}{2} + U^2 h \left(1 + \frac{h}{4} \frac{d^2 h}{dx^2} + \frac{h}{2} \frac{d^2 z_b}{dx^2} \right). \quad (2.127)$$

Equation (2.127) is based on a linear pressure distribution with depth. If the parabolic pressure distribution due to Serre (1953) is used instead, the factor (1/4) in the water curvature term must be replaced by (1/3), leading to the theoretical equation used by Engelund and Hansen (1966)

$$M = g \frac{h^2}{2} + U^2 h \left(1 + \frac{h}{3} \frac{d^2 h}{dx^2} + \frac{h}{2} \frac{d^2 z_b}{dx^2} \right). \quad (2.128)$$

Note that the more general Eq. (2.122) for the momentum flux M is accounting for both unsteadiness and bed-load transport. Although coastal engineering applications are not within the scope of this book, the equations presented are of applicability in this branch of hydraulics too. The propagation of solitary waves over submerged obstacles, e.g., an island, is an application in the realm of coastal engineering; it was so developed by Seabra-Santos et al. (1987). Consider the more general theory by Serre (1953). The 1D unsteady x -momentum equation, in which the stress terms are neglected (potential flow), is, from Eq. (2.28),

$$\frac{\partial}{\partial t}(Uh) + \frac{\partial M}{\partial x} = -\frac{p_b}{\rho} \frac{\partial z_b}{\partial x}, \quad (2.129)$$

where

$$M = hU^2 + \int_{z_b}^{z_s} \frac{p}{\rho} dz. \quad (2.130)$$

The vertical velocity for unsteady 1D flowing over curved terrain is obtained from Eq. (2.37),

$$\begin{aligned} w &= -\frac{\partial}{\partial x}[U(z - z_b)] = -\frac{\partial}{\partial x} \left[\frac{\partial U}{\partial x}(z - z_b) - U \frac{\partial z_b}{\partial x} \right] \\ &= -\frac{\partial U}{\partial x}(z - z_b) + U \frac{\partial z_b}{\partial x}. \end{aligned} \quad (2.131)$$

Similarly, the expression for the pressure is, from Eq. (2.40),

$$p = \rho g(z_s - z) + \rho \frac{\partial}{\partial t} \int_z^{z_s} w dz' + \rho \frac{\partial}{\partial x} \left[U \int_z^{z_s} w dz' \right] - \rho w^2. \quad (2.132)$$

Computing the integral

$$\int_z^{z_s} w dz' = -\frac{\partial U}{\partial x} \frac{(h^2 - \eta^2)}{2} + U \frac{\partial z_b}{\partial x} (h - \eta), \quad (2.133)$$

and inserting Eqs. (2.131) and (2.133) into Eq. (2.132), the pressure distribution is obtained with similar steps to those used to obtain Eq. (2.67).

For illustrative purposes, an alternative procedure is presented here to obtain the flow momentum M without computing the distribution $p(z)$. The vertical equation of motion for an inviscid fluid is

$$\frac{Dw}{Dt} = \frac{\partial w}{\partial t} + u \frac{\partial w}{\partial x} + v \frac{\partial w}{\partial y} + w \frac{\partial w}{\partial z} = -\frac{1}{\rho} \frac{\partial p}{\partial z} - g. \quad (2.134)$$

Multiplying Eq. (2.134) by $\eta = z - z_b$ gives

$$\eta \frac{Dw}{Dt} = -\frac{1}{\rho} \eta \frac{\partial p}{\partial z} - g\eta, \quad (2.135)$$

or

$$\eta \frac{Dw}{Dt} = -\frac{1}{\rho} \left[\frac{\partial}{\partial z} (p\eta) - p \right] - g\eta. \quad (2.136)$$

Integrating Eq. (2.136) over the flow depth yields

$$\int_{z_b}^{z_s} \eta \frac{Dw}{Dt} dz = -\frac{1}{\rho} \int_{z_b}^{z_s} \frac{\partial}{\partial z} (p\eta) dz + \frac{1}{\rho} \int_{z_b}^{z_s} p dz - \int_{z_b}^{z_s} g\eta dz, \quad (2.137)$$

or after the evaluation of the integrals

$$\frac{1}{\rho} \int_{z_b}^{z_s} p dz = g \frac{h^2}{2} + \int_{z_b}^{z_s} \eta \frac{Dw}{Dt} dz. \quad (2.138)$$

Equation (2.138) is an exact depth-integrated identity, useful for the exact definition of the momentum flux if one does not wish to compute the pressure distribution from Eq. (2.132). Equation (2.130) is rewritten with the aid of Eq. (2.138) as

$$M = hU^2 + g \frac{h^2}{2} + \int_{z_b}^{z_s} \eta \frac{Dw}{Dt} dz. \quad (2.139)$$

Now, Dw/Dt is for flow in a vertical plane

$$\frac{Dw}{Dt} = \frac{\partial w}{\partial t} + u \frac{\partial w}{\partial x} + w \frac{\partial w}{\partial z}. \quad (2.140)$$

Using Eq. (2.131) one gets

$$\begin{aligned} \frac{\partial w}{\partial t} &= -\frac{\partial^2 U}{\partial x \partial t} (z - z_b) + \frac{\partial U}{\partial t} \frac{\partial z_b}{\partial x}, \\ \frac{\partial w}{\partial z} &= -\frac{\partial U}{\partial x}, \\ \frac{\partial w}{\partial x} &= -\frac{\partial^2 U}{\partial x^2} (z - z_b) + 2 \frac{\partial U}{\partial x} \frac{\partial z_b}{\partial x} + U \frac{\partial^2 z_b}{\partial x^2}, \end{aligned} \quad (2.141)$$

from which Eq. (2.140) takes the form

$$\frac{Dw}{Dt} = \left[\left(\frac{\partial U}{\partial x} \right)^2 - \frac{\partial^2 U}{\partial x \partial t} - U \frac{\partial^2 U}{\partial x^2} \right] \eta + \frac{\partial U}{\partial t} \frac{\partial z_b}{\partial x} + U \frac{\partial U}{\partial x} \frac{\partial z_b}{\partial x} + U^2 \frac{\partial^2 z_b}{\partial x^2}. \quad (2.142)$$

Inserting Eq. (2.142) into Eq. (2.139) results in the momentum flow function

$$M = U^2 h + g \frac{h^2}{2} + (U_x^2 - U_{xt} - UU_{xx}) \frac{h^3}{3} + \left(\frac{\partial U}{\partial t} \frac{\partial z_b}{\partial x} + U \frac{\partial U}{\partial x} \frac{\partial z_b}{\partial x} + U^2 \frac{\partial^2 z_b}{\partial x^2} \right) \frac{h^2}{2}. \quad (2.143)$$

The bottom pressure is computed by integrating Eq. (2.134) and inserting Eq. (2.142) as

$$\begin{aligned} \frac{p_b}{\rho} &= gh + \int_{z_b}^{z_s} \frac{Dw}{Dt} dz \\ &= gh + (U_x^2 - U_{xt} - UU_{xx}) \frac{h^2}{2} + \left(\frac{\partial U}{\partial t} \frac{\partial z_b}{\partial x} + U \frac{\partial U}{\partial x} \frac{\partial z_b}{\partial x} + U^2 \frac{\partial^2 z_b}{\partial x^2} \right) h. \end{aligned} \quad (2.144)$$

Seabra-Santos et al. (1987) numerically solved Eqs. (2.129), (2.143), and (2.144) coupled with the continuity equation, finding an accurate description of solitary wave propagation over submerged obstacles. This simplified model is, therefore, a particular case of the general theory developed here.

2.6 Numerical Methods for Boussinesq-Type Models

2.6.1 Unsteady Flow Simulations

Simulation of unsteady flows using depth-averaged models generally requires numerical solutions. The numerical technique used to solve the mathematical equations describing the physical system must be robust and stable. Water flows over irregular topography experiences changes in the flow regimes due to moving shocks (Vreugdenhil 1994; Toro 1997, 2001; Chaudhry 2008; Kim et al. 2009). A key issue for numerical modeling is that the system of equations must be written in conservative form, as done in Eq. (2.33), because shocks are otherwise not captured. The unsteady non-hydrostatic flow equations were solved using finite difference methods for applications involving water wave propagation, in particular by Peregrine (1966, 1967), Seabra-Santos et al. (1987), Antunes do Carmo et al. (1993), Wei et al. (1995), and Mohapatra and Chaudhry (2004), among others. The unsteady non-hydrostatic flow equations were solved using a finite element method by Khan and Steffler (1996a, b) for applications in hydraulic structures. However, the finite volume method appears to be the technique of most frequent use in free surface flow modeling (Le Veque 2002; Toro 2001; Kim et al. 2009; Denlinger and O'Connell 2008), even though it is sometimes coupled in a hybrid way, either with finite difference (Kim et al. 2009), or finite element methods, i.e., the discontinuous method of Galerkin (Khan and Lai 2014). In this section, a practical introduction to finite volume methods for shallow water flows is presented. For fundamental issues or advanced topics, the books of Toro (1997, 2001) or Le Veque (2002) are recommended.

Consider 1D unsteady water flows over a curved and rigid bottom as described for instance by Denlinger and O'Connell (2008). The conservation laws has the form

$$\frac{\partial \mathbf{U}}{\partial t} + \frac{\partial \mathbf{F}}{\partial x} = \mathbf{S}. \quad (2.145)$$

Here, \mathbf{U} is the vector of the conserved variables, \mathbf{F} is the flux vector, and \mathbf{S} the source term vector, given by

$$\mathbf{U} = \begin{pmatrix} h \\ hU \end{pmatrix}, \quad \mathbf{F} = \begin{pmatrix} hU \\ hU^2 + \frac{1}{2}g'h^2 \end{pmatrix}, \quad \mathbf{S} = \begin{pmatrix} 0 \\ -g'h \frac{\partial z_b}{\partial x} - \frac{\tau_b}{\rho} \end{pmatrix}. \quad (2.146)$$

Furthermore, the enhanced gravity for 1D flows is given by

$$g' = g + \frac{D\bar{w}}{Dt} = g + \frac{\partial \bar{w}}{\partial t} + U \frac{\partial \bar{w}}{\partial x}, \quad (2.147)$$

in which the depth-averaged vertical velocity for flows over a rigid bed is given by

$$\bar{w} = \frac{1}{2} \left(\frac{\partial h}{\partial t} + U \frac{\partial h}{\partial x} \right) + U \frac{\partial z_b}{\partial x} = w_b - h \frac{\partial U}{\partial x}, \quad w_b = U \frac{\partial z_b}{\partial x}. \quad (2.148)$$

The differential Eq. (2.145) is valid in the zones of the computational domain with smooth or continuous solutions, but it does not apply at discontinuous portions like moving shocks. Therefore, Eq. (2.145) is integrated over a control volume in the x - t plane as

$$\iint \left(\frac{\partial \mathbf{U}}{\partial t} + \frac{\partial \mathbf{F}}{\partial x} \right) dx dt = \iint \mathbf{S} dx dt. \quad (2.149)$$

The integral Eq. (2.149) permits the computation of both continuous and discontinuous solutions as shocks. It is the base of the finite volume method. For a rectangular control volume in the x - t plane (Fig. 2.10), one can write

$$\int_t^{t+\Delta t} \int_{x_{i-1/2}}^{x_{i+1/2}} \left(\frac{\partial \mathbf{U}}{\partial t} + \frac{\partial \mathbf{F}}{\partial x} \right) dx dt = \int_{x_{i-1/2}}^{x_{i+1/2}} dx \int_t^{t+\Delta t} \frac{\partial \mathbf{U}}{\partial t} dt + \int_t^{t+\Delta t} dt \int_{x_{i-1/2}}^{x_{i+1/2}} \frac{\partial \mathbf{F}}{\partial x} dx = \iint \mathbf{S} dx dt \quad (2.150)$$

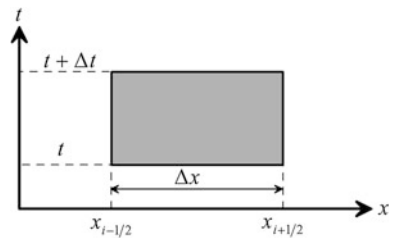
Here, i is the cell index in the x -direction, and $i + 1/2$ the interface between cells i and $i + 1$. The integral of Eq. (2.150) is then exactly given by (Toro 1997, 2001)

$$\int_{x_{i-1/2}}^{x_{i+1/2}} [\mathbf{U}(t + \Delta t) - \mathbf{U}(t)] dx + \int_t^{t+\Delta t} [\mathbf{F}(x_{i+1/2}) - \mathbf{F}(x_{i-1/2})] dt = \iint \mathbf{S} dx dt. \quad (2.151)$$

Note that despite the notation is made with reference to the cell index i , and corresponding interfaces, no numerical approximations are invoked in Eq. (2.151).

Let temporal and spatial average values be

Fig. 2.10 Control volume in x - t plane



$$\begin{aligned}
\mathbf{F}_{i+1/2} &= \frac{1}{\Delta t} \int_t^{t+\Delta t} \mathbf{F}(x_{i+1/2}, t) dt, \\
\mathbf{F}_{i-1/2} &= \frac{1}{\Delta t} \int_t^{t+\Delta t} \mathbf{F}(x_{i-1/2}, t) dt, \\
\mathbf{U}_i^{n+1} &= \frac{1}{\Delta x} \int_{x_{i-1/2}}^{x_{i-1/2} + \Delta x} \mathbf{U}(x, t + \Delta t) dx, \\
\mathbf{U}_i^n &= \frac{1}{\Delta x} \int_{x_{i-1/2}}^{x_{i-1/2} + \Delta x} \mathbf{U}(x, t) dx, \\
\mathbf{S}_i &= \frac{1}{\Delta x \Delta t} \iint \mathbf{S} dx dt.
\end{aligned} \tag{2.152}$$

For the quadrilateral control volume in the x - t plane as shown in Fig. 2.10, the conservative Eq. (2.151) reads exactly, using Eq. (2.152) for time and space averages,

$$\mathbf{U}_i^{n+1} = \mathbf{U}_i^n - \frac{\Delta t}{\Delta x} (\mathbf{F}_{i+1/2} - \mathbf{F}_{i-1/2}) + \Delta t \mathbf{S}_i. \tag{2.153}$$

In the finite volume method, the computational domain is divided into a number of control volumes in the x - t plane (Fig. 2.11), where Eq. (2.153) is applied. Here, $\mathbf{F}_{i+1/2}$ is the numerical flux across the interface between cells i and $i + 1$. Again, no numerical approximations are introduced in Eq. (2.153), but its formulation is presented in the usual form suitable for developing numerical schemes.

In practice, the source terms \mathbf{S}_i and the fluxes $\mathbf{F}_{i+1/2}$ are evaluated at a suitable time level that depends on the specific method applied (Toro 1997, 2001), thereby introducing numerical approximations. Usually, explicit schemes are employed. Shock-capturing finite volume solutions using the Godunov upwind method assisted by robust Riemann solvers (approximate or exact) are well established today as accurate solvers of shallow water flows (Toro 2001; LeVeque 2002;

Fig. 2.11 Intercell fluxes

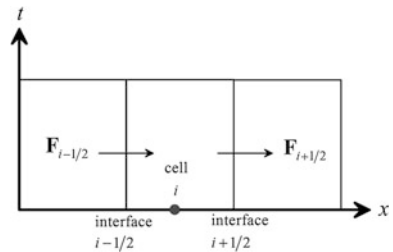


Fig. 2.12 Piecewise approximation using cell-averaged values

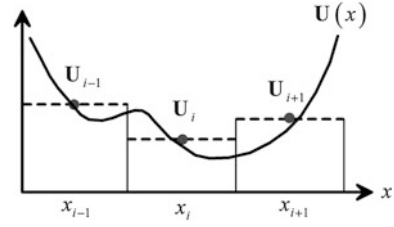
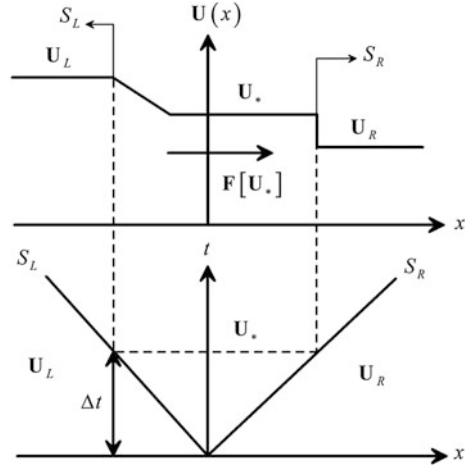


Fig. 2.13 Riemann problem solution structure for left-going rarefaction wave and right going shock front



Denlinger and O'Connell 2008 among others). In the Godunov upwind method, the actual solution $U(x)$ at time t is approximated by the cell-averaged values within each cell (Fig. 2.12).

Between two adjacent cells, there is a discontinuity in U , giving rise to a number of local Riemann problems at each cell interface. Consider two states U_L and U_R separated at the initial time, at a generic interface between two cells. This is by definition a local Riemann problem, and a number of wave patterns may evolve after a time Δt . In Fig. 2.13, the typical case with a left-going rarefaction wave and right-going shock front is presented (note the local system of reference with x -origin at the cell interface). The shock front and rarefaction wave propagate with signal speeds S_R and S_L , respectively.

The constant state region just behind the shock front (star region) is denoted as U_* . The numerical flux crossing the original discontinuity at $x = 0$ is F , which is needed to apply Eq. (2.153). Note that the start region in the Riemann problem is essentially a steady-state zone where the conserved variables are U_* , which is a part of the total (local) Riemann solution $U(x)$ after time Δt . Therefore, the numerical flux crossing the t -axis ($x = 0$) in the Riemann problem is also a constant, so that the intercell flux is exactly evaluated based on the Riemann solution at $x = 0$ as

$$\mathbf{F}_{i+1/2} = \underbrace{\frac{1}{\Delta t} \int_t^{t+\Delta t} \mathbf{F}(x_{i+1/2}, t) dt}_{\text{global system of reference}} = \underbrace{\frac{1}{\Delta t} \int_0^{\Delta t} \mathbf{F}(0, t) dt}_{\text{local system of reference}} = \mathbf{F}[\mathbf{U}(x=0)] = \mathbf{F}(\mathbf{U}_*). \quad (2.154)$$

Therefore, the numerical flux at each interface is computed based on the solution of the local Riemann problem $\mathbf{U}(x)$ at this interface, evaluated at $x = 0$.

The solution of the Riemann problem may be conducted exactly, but resort to a numerical method to solve the resulting implicit, nonlinear equation is required. Thus, approximate (explicit) Riemann solvers use a simplified representation of the wave structure as shown in Fig. 2.13. Here, the Harten-Lax-van Leer (HLL) approximate Riemann solver is presented, suitable for 1D depth-averaged water flow equations. It approximates the intercell numerical flux as (Toro 2001)

$$\mathbf{F}_{i+1/2} = \begin{cases} \mathbf{F}_L & \text{if } S_L \geq 0, \\ \frac{S_R \mathbf{F}_L - S_L \mathbf{F}_R + S_R S_L (\mathbf{U}_R - \mathbf{U}_L)}{S_R - S_L}, & \text{if } S_L \leq 0 \leq S_R, \\ \mathbf{F}_R & \text{if } S_R \leq 0. \end{cases} \quad (2.155)$$

Here, \mathbf{F}_L and \mathbf{F}_R are the fluxes computed at states L and R . Basically, the method assumes that the left and right waves are discontinuities, and between them there is a constant-state solution denoted as \mathbf{U}_{HLL} . Figure 2.14 illustrates wave propagation cases for the HLL Riemann solver. For a detailed theoretical derivation of the HLL equations, see Toro (1997, 2001). Robust wave speed estimates S_L and S_R are given by (Toro 2001)

$$S_L = U_L - a_L q_L; \quad S_R = U_R + a_R q_R. \quad (2.156)$$

Here $a = (g'h)^{1/2}$, and q_K ($K = L, R$) is

$$q_K = \begin{cases} \left[\frac{1}{2} \left(\frac{h_*(h_* + h_K)}{h_K^2} \right) \right]^{1/2} & h_* > h_K, \\ 1 & h_* \leq h_K. \end{cases} \quad (2.157)$$

Note the use of the enhanced gravity in the Riemann problem (Denlinger and Iverson 2004; Denlinger and O'Connell 2008), and, thus, the inclusion of the non-hydrostatic pressure in the computation of numerical fluxes. The flow depth at the star region of the Riemann problem at each interface h_* is

$$h_* = \frac{1}{g} \left(\frac{1}{2} (a_L + a_R) + \frac{1}{4} (U_L - U_R) \right)^2. \quad (2.158)$$

For a channel reach, discretized into a number of finite volumes, the computation of the intercell numerical flux $\mathbf{F}_{i+1/2}$ amounts to solve several local Riemann problems,

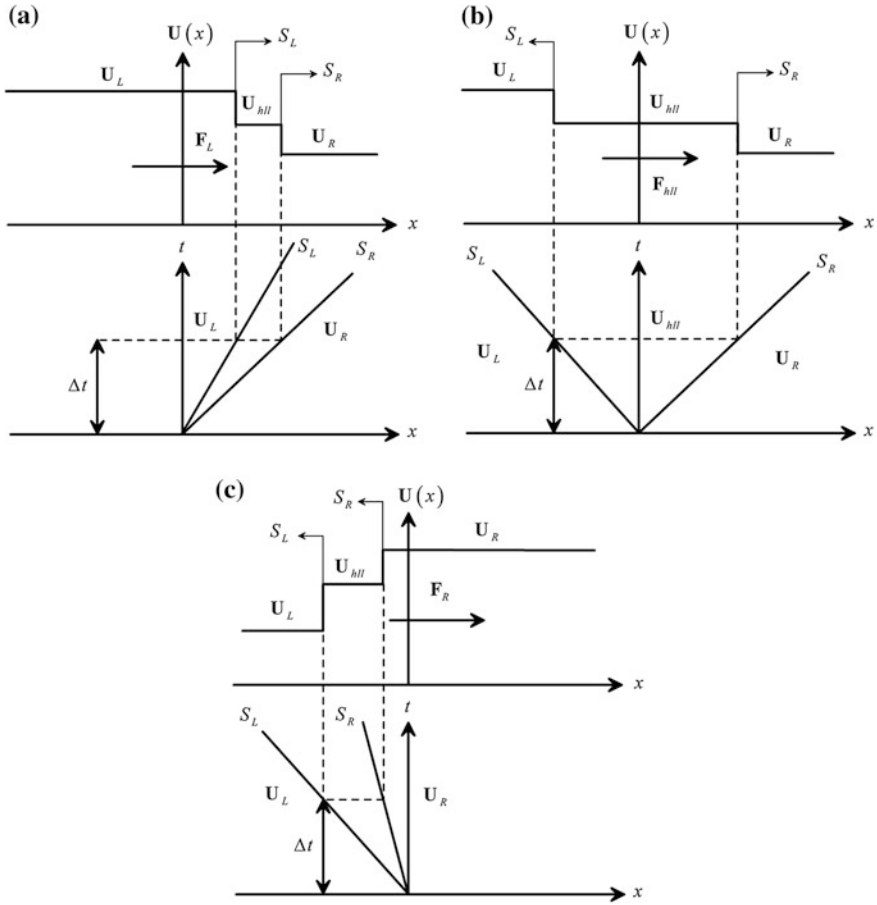
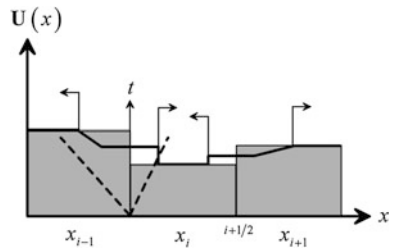


Fig. 2.14 Wave propagation cases of HLL approximate Riemann solver. Cases **a–c** represent Eq. (2.155)

Fig. 2.15 Wave propagation at cell interfaces with (thick lines) as instantaneous $U(x)$ profile and (dashed lines) x - t rarefaction wave and shock front paths at interface $i - 1/2$



one between each adjacent cells. As a result, the evolution of \mathbf{U} in the computational domain accounts for the wave propagation conditions at interfaces (Fig. 2.15). Therefore, the method is of upwind type, i.e., the wave propagation

information is used to update the conserved variables in time. This method, first-order accurate in both space and time, is essentially the Godunov first-order upwind method. However, high-order accuracy is sometimes advisable. To obtain second-order accuracy in space, a polynomial reconstruction is made within each cell, sometimes linear. Linear slopes resulting from the reconstructed solution must be limited to avoid spurious oscillations near discontinuities.

For stability in time of the explicit scheme, the Courant–Friedrichs–Lewy number **CFL** must be less than unity. The time step Δt is then determined at time level n using the equation

$$\Delta t = \frac{\Delta x}{\max(|U_i^n| + (gh_i^n)^{1/2})} \text{CFL}. \quad (2.159)$$

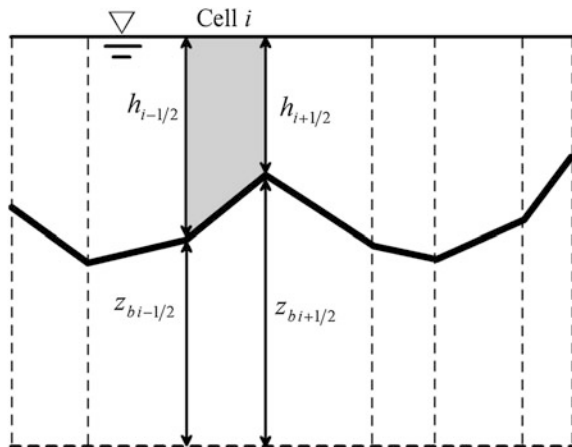
Here, Δt and Δx are the step sizes in the x - and t -directions, respectively. Details are found in Toro (1997, 2001).

The computation of shallow water flows over variable topography must be conducted using a well-balanced scheme (Toro 2001). It implies that once a discretization is applied to the source terms \mathbf{S}_i , the time evolution of the conserved variables must reach a stable steady state $\mathbf{U}_i^{n+1} = \mathbf{U}_i^n$ if afforded by the boundary conditions. The asymptotic steady-state version of Eq. (2.153) then takes the form

$$(\mathbf{F}_{i+1/2} - \mathbf{F}_{i-1/2}) + \Delta x \mathbf{S}_i = \mathbf{0}. \quad (2.160)$$

It may be regarded as an identity that is verified only if the discretization of \mathbf{S} is correctly implemented. Consider as example static water over variable topography (Fig. 2.16). The imbalance of intercell fluxes at cell i is then given by the hydrostatic forces as

Fig. 2.16 Static water over variable topography



$$F_{i+1/2} - F_{i-1/2} = g \frac{(h_{i+1/2}^2 - h_{i-1/2}^2)}{2} = g \frac{(h_{i+1/2} - h_{i-1/2})(h_{i+1/2} + h_{i-1/2})}{2}. \quad (2.161)$$

The compatible discretization of the bed slope source term to verify Eq. (2.160) due to the condition $h + z_b = \text{const.}$ is

$$S_i = gh_i \left(\frac{\partial z_b}{\partial x} \right)_i = g \frac{(h_{i+1/2} + h_{i-1/2})}{2} \frac{(z_{bi+1/2} - z_{bi-1/2})}{\Delta x}. \quad (2.162)$$

Other discretizations of the bed slope source term will generate unphysical numerical flux.

In general, numerical difficulties are introduced by dispersion terms in non-hydrostatic depth-averaged models. As an illustrative example, consider Eqs. (2.48)–(2.49). Assume that they are discretized using finite difference discretization (Chaudhry 2008). Finite differencing to second-order accuracy of the first-order derivative $\partial U / \partial x = (U_{i+1} - U_{i-1}) / (2\Delta x) + O(\Delta x^2)$ produces in the Saint-Venant terms truncation errors proportional to U_{xxx} . These errors will have mathematically the same form as physical dispersive terms (Abbott 1979; Wei and Kirby 1995), just as those originating from expanding the gradient $\partial(h^3 U U_{xx} / 3) / \partial x$. If no counter measures are taken to reduce truncation errors, physical dispersive effects are masked by numerical oscillations. Thus, higher-order differencing of leading order hydrostatic (Saint-Venant) terms is required to guarantee that physical dispersion effects are not masked by spurious numerical oscillations associated with truncation errors (Wei and Kirby 1995). Ideally, these problems disappear with a computational mesh, if $\Delta x \rightarrow 0$ and $\Delta y \rightarrow 0$. However, this is not practical, so that the control of truncation errors is necessary for usual meshes. Kim et al. (2009) provide a useful reference, given the account of all these issues in a finite volume model. Their modified finite volume method for dispersive systems consists in substituting the Euler time stepping by a fourth-order accurate time stepping method, composed of a predictor step using a third-order Adams–Bashforth formula and an iterative corrector using a fourth-order Adam–Moulton formula. The treatment of the leading order hydrostatic terms was done using a fourth-order accurate MUSCL TVD procedure for reconstruction of interface values and a HLLC Riemann solver to compute fluxes. Prior to the application of the finite volume solution, the vector \mathbf{U} is mathematically replaced by an auxiliary vector that includes terms with spatial derivatives, to eliminate time derivatives (contained in mixed terms such as U_{xt}) from the vectors \mathbf{F} and \mathbf{G} . The solution is then performed for auxiliary variables, and the vector \mathbf{U} is determined by discretizing the spatial derivatives to second-order accuracy, leading to tridiagonal systems for determining \mathbf{U} . For high-resolution finite volume solutions of non-hydrostatic water wave problems, see Cienfuegos et al. (2006), Kim et al. (2009), and Cantero-Chinchilla et al. (2016a, b).

2.6.2 Steady Flow Simulations

A great variety of non-hydrostatic problems can be considered under steady flow conditions. According to Roache (1976), a steady flow condition may be regained as limiting asymptotic state after a transient flow computation. Khan and Steffler (1996a, b) pursued this approach and computed steady flows in curved bed structures using unsteady flow computations. Another option is to directly solve the steady-state version of the governing equations. Generally, this leads to a system of ordinary differential equations (ODEs), typically reduced to a single third-order ODE, as shown in the next example. Consider based on Eqs. (2.62), (2.68), and (2.69), the flow over a curved bed as given by the ODE

$$\begin{aligned} \frac{d}{dx} \left[\frac{h^2}{2} + \frac{q^2}{gh} \left(1 + \frac{hh_{xx} - h_x^2}{3} + \frac{hz_{bxx}}{2} - \frac{h_x z_{bx}}{2} \right) \right] \\ = - \left[h + \frac{q^2}{2g} (2hz_{bxx} + hh_{xx} - h_x^2 - 2h_x z_{bx}) \right] z_{bx}. \end{aligned} \quad (2.163)$$

Neglecting second-order products of derivatives of h and z_b , Eq. (2.163) is simplified to

$$\frac{q^2}{g} \left(\frac{1}{3} \frac{d^3 h}{dx^3} + \frac{1}{2} \frac{d^2 z_b}{dx^2} \right) + \left(h - \frac{q^2}{gh^2} \right) \frac{dh}{dx} = -h \frac{dz_b}{dx}. \quad (2.164)$$

This closely resembles the original Boussinesq momentum equation for curved beds (Boussinesq 1877). The solution of a steady Boussinesq equation is a boundary-value problem. Equation (2.164) is a third-order ODE, so that three boundary conditions are needed. It can be solved using shooting methods (e.g., by resort to Runge–Kutta solvers), but this approach requires high precision in setting the conditions at the upstream boundary section (Hager and Hager 1985; Fenton 1996). Typically, h , dh/dx , and d^2h/dx^2 are prescribed at the shooting boundary section. There, in most cases, $d^2h/dx^2 = 0$, but dh/dx must be iteratively determined with the shooting method until the downstream boundary condition at the end section of the computational domain is satisfied. This method is simple despite the high accuracy needed in the computation of dh/dx at the shooting section. An alternative is to solve the problem using a finite difference approximation of the derivatives in Eq. (2.164). In this case, the values of the flow depth prescribed at the two boundary sections of the computational domain, plus dh/dx at one of these sections, are directly incorporated into the mathematical model. The numerical method in this case is more complicated than in the shooting approach, given that a system of nonlinear implicit equations results to be solved iteratively to compute the water depths at the nodes of the finite difference mesh, by any numerical technique, as the Newton–Raphson or Secant methods. This approach was adopted

by Hosoda and Tada (1994), Zerihun and Fenton (2006, 2007), and Castro-Orgaz and Hager (2009). Zhu and Lawrence (1998) solved alternatively the boundary-value problem using a collocation method.

2.7 Higher-Order Equations

2.7.1 Fawer-Type Equations

The theory based on Serre's work (1953) may be regarded as accurate for most open-channel flow problems. However, higher-order models may be needed in some instances. These are obtained by taking higher-order approximations for the velocity and pressure distributions to be used in the general depth-averaged equations. While this may be done using mathematical techniques used in fluid mechanics, such as the expansion of the flow variables using Taylor series (Mei 1983) or a perturbation procedure (Peregrine 1967), the costs involved in the integration of a higher-order model will be paid by an increase in the order of differentiation in the system of PDEs (Madsen and Schäffer 1998). Fawer (1937) produced an interesting approach to increase the resolution details of Boussinesq-type equations in the vertical direction without further increasing the order of differentiation (usually the higher-order spatial derivative is limited to third order). He proposed to use an interpolation equation for the streamline curvature κ in the vertical direction of the form

$$\kappa = \kappa_b + (\kappa_s - \kappa_b) \left(\frac{z}{h} \right)^K. \quad (2.165)$$

Here, κ_s is the radius of curvature at the free surface, κ_b the radius of curvature at the channel bottom, and K is a free parameter to be determined. This theory will extensively be described in Chap. 3; here, only the main aspects are discussed as a means of comparison with Serre's approach (1953).

Su and Gardner (1969) made an interesting development to be used for this purpose. They formulated the momentum function M for unsteady flows as

$$M = \int_0^h u^2 dz + g \frac{h^2}{2} + \int_0^h \frac{Dw}{Dt} z dz, \quad (2.166)$$

where $w(x, z, t)$ is the vertical velocity and

$$\frac{Dw}{Dt}(x, z, t) = \frac{\partial w}{\partial t} + u \frac{\partial w}{\partial x} + w \frac{\partial w}{\partial z}. \quad (2.167)$$

Using an irrotational solution of the velocity and pressure fields, they found that the correction for the non-uniformity of u over the depth in Eq. (2.166) is proportional to $[\partial^2 U / \partial x^2]^2$ and thus of higher order. Therefore, the momentum flux is $U^2 h$. Then, they essentially arrived at Serre's equation for 1D flows based on the irrotational flow theory

$$M = hU^2 + g \frac{h^2}{2} + (U_x^2 - U_{xt} - UU_{xx}) \frac{h^3}{3}. \quad (2.168)$$

If a mean acceleration term over the depth is taken using the depth-averaged vertical velocity \bar{w} , then Eq. (2.166) yields

$$M = \int_0^h u^2 dz + g \frac{h^2}{2} + \int_0^h \frac{Dw}{Dt} z dz = \int_0^h U^2 dz + g \frac{h^2}{2} + \int_0^h \frac{D\bar{w}}{Dt} z dz = U^2 h + g' \frac{h^2}{2}, \quad (2.169)$$

where

$$\frac{D\bar{w}}{Dt} = \frac{\partial \bar{w}}{\partial t} + U \frac{\partial \bar{w}}{\partial x}. \quad (2.170)$$

This approach was pursued by Denlinger and Iverson (2004) and may be regarded as a depth-averaged approximation to the integral result of Su and Gardner (1969). Intuitively, Eq. (2.166) reveals that a method to produce higher-order flow equations relies on improving the estimation of the vertical acceleration term of the momentum function. The linear vertical velocity profile of Serre (1953),

$$w = -\frac{\partial U}{\partial x} z, \quad (2.171)$$

is closely related to a linear variation in the streamline curvature, i.e., Eq. (2.165) with $K = 1$,

$$\kappa = \kappa_b + (\kappa_s - \kappa_b) \left(\frac{z}{h} \right), \quad (2.172)$$

which is similar to the theory of Matthew (1963). Therefore, improving the estimation of Dw/Dt amounts to use a value of K different from unity. Fenton (1996) and Fenton and Zerihun (2007) produced such an illustrative Fawer-type theory. For 1D steady flow over a curved bed, they expressed the vertical pressure gradient as

$$\frac{1}{\rho} \frac{\partial p}{\partial z} = -g - \frac{Dw}{Dt}. \quad (2.173)$$

Moreover, they estimated Dw/Dt in a vertical section using an average value, producing an approximation, with $\bar{\kappa}$ as depth-averaged streamline curvature and g' as the corresponding enhanced gravity in the section, as

$$\frac{1}{\rho} \frac{\partial p}{\partial z} = -g - U^2 \bar{\kappa} = -g'. \quad (2.174)$$

Therefore, the non-hydrostatic correction in Eq. (2.174) is interpreted as a depth-averaged centrifugal acceleration contribution (Fenton 1996), which essentially corresponds to the use of an enhanced gravity (Denlinger and Iverson 2004). The parameter $\bar{\kappa}$ may be interpolated between the curvature values at the free surface, z_s , and at the channel bed, z_b , as

$$\bar{\kappa} = (1 - \omega)\kappa_b + \omega\kappa_s \approx \frac{\partial^2 z_b}{\partial x^2} + \omega \frac{\partial^2 h}{\partial x^2}. \quad (2.175)$$

Here, ω is a weighting factor to distribute the contributions of the bed and free surface curvatures on the depth-averaged centrifugal acceleration; slope contributions are neglected. The corresponding momentum function is then

$$\begin{aligned} M &= \int_0^h \left(u^2 + \frac{p}{\rho} \right) dz = U^2 h + g \frac{h^2}{2} \left(1 + \frac{U^2}{g} \bar{\kappa} \right) = g \frac{h^2}{2} + U^2 h \left(1 + \frac{\bar{\kappa} h}{2} \right) \\ &= g \frac{h^2}{2} + U^2 h \left(1 + \frac{\omega h h_{xx}}{2} + \frac{h z_{bxx}}{2} \right). \end{aligned} \quad (2.176)$$

In Chap. 3, it will be demonstrated that using Fawer's Eq. (2.165), the momentum function reads, if slope effects are neglected,

$$M = g \frac{h^2}{2} + U^2 h \left(1 + \frac{h h_{xx}}{K+2} + \frac{h z_{bxx}}{2} \right). \quad (2.177)$$

Comparing Eqs. (2.176) and (2.177) gives the identity

$$\omega = \frac{2}{K+2}. \quad (2.178)$$

For $\omega = 2/3$ (Fenton and Zerihun 2007), Eq. (2.176) gives the basic result of the original Boussinesq (1877) theory, namely

$$M = g \frac{h^2}{2} + U^2 h \left(1 + \frac{h h_{xx}}{3} + \frac{h z_{bxx}}{2} \right). \quad (2.179)$$

The compatibility value of Fawer's theory is then $K = 1$ from Eq. (2.178), as used by Matthew (1963). Inserting Eq. (2.179) into the streamwise momentum balance,

$$\frac{dM}{dx} = gh(S_o - S_f), \quad (2.180)$$

produces the ODE (note that the momentum velocity correction coefficient is unity)

$$\frac{U^2 h^2}{g} \left(\frac{1}{3} \frac{d^3 h}{dx^3} - \frac{1}{2} \frac{d^2 S_o}{dx^2} \right) + \left(h - \frac{U^2}{g} \right) \frac{dh}{dx} = h(S_o - S_f). \quad (2.181)$$

This was originally developed by Boussinesq (1877) and rederived by Fenton and Zerihun (2007), with S_o as the bottom slope and S_f as the friction slope.

Once the main ingredient of Fawer's theory is elucidated, an enhanced 1D unsteady flow model is produced to illustrate how higher-order equations may be formulated. Serre's (1953) theory is based on a parabolic pressure distribution (Castro-Orgaz et al. 2015), whereas Khan and Steffler (1996a, b) and Denlinger and Iverson (2004) prescribed a linear pressure profile to the flow equations. A general interpolation function for the pressure profile follows Fawer (1937) as

$$p = \rho gh \left(1 - \frac{z}{h} \right) + p_1 \left[1 - \left(\frac{z}{h} \right)^K \right]. \quad (2.182)$$

Here, the free surface pressure vanishes at $z/h = 1$, and the bed pressure in excess of the hydrostatic pressure is p_1 (Khan and Steffler 1996a, b), namely

$$p_1 = \rho \frac{\partial}{\partial t} (\bar{w}h) + \rho \frac{\partial}{\partial x} (\bar{w}Uh). \quad (2.183)$$

Using Eq. (2.182), the momentum function is then

$$M = \int_0^h \left(u^2 + \frac{p}{\rho} \right) dz = U^2 h + g \frac{h^2}{2} + \frac{K}{K+1} \frac{p_1 h}{\rho}. \quad (2.184)$$

For $K = 1$, this expression gives the momentum function of Khan and Steffler's Boussinesq-type model, whereas $K = 2$ results in Serre's theory. For flows over a horizontal bed, Eqs. (2.183)–(2.184) may be combined, using Eq. (2.144), to yield

$$\begin{aligned} M &= U^2 h + g \frac{h^2}{2} + \frac{K}{K+1} \frac{p_1 h}{\rho} = U^2 h + g \frac{h^2}{2} + \frac{K}{K+1} \left[(U_x^2 - U_{xt} - UU_{xx}) \frac{h^2}{2} \right] h \\ &= U^2 h + g \frac{h^2}{2} + (U_x^2 - U_{xt} - UU_{xx}) \frac{h^3}{3\lambda}, \end{aligned} \quad (2.185)$$

where the auxiliary variable λ , affecting the non-hydrostatic term, is (Castro-Orgaz et al. 2015)

$$\lambda = \frac{2K+1}{3K}. \quad (2.186)$$

The specific value of K for a given flow problem may be found by fitting the depth-averaged model results to experimental data, or to a 2D solution in a certain range of applications (Fawer 1937).

2.7.2 Moment Equations

Steffler and Jin (1993) devised an important method to better recover vertical resolution details in depth-averaged models. Essentially, they produced general 1D depth-averaged momentum equations in the horizontal and vertical directions, in addition to the well-known continuity equation. If arbitrary distributions of (u, w, p) are set into the depth-averaged equations, a number of free parameters remain undetermined. While for specific cases it may be possible to find approximate predictors based on experimental observations, the idea of the method is to produce an additional set of PDEs, one more for each undetermined free parameter, given that the number of PDEs in the system must be compatible with the number of unknown functions. The standard depth-averaged process described in this chapter may be regarded as a weighted residual method with unit weighting functions (Steffler and Jin 1993). Additional independent depth-averaged equations are determined using weighting functions including collocation, Galerkin, and moment methods. Steffler and Jin (1993) used the weighting function

$$f = 2 \frac{z - \bar{z}}{h}, \quad \bar{z} = z_b + \frac{h}{2}. \quad (2.187)$$

The continuity, horizontal, and vertical momentum equations are then multiplied by f and depth-integrated, producing three moment equations. As to the distributions of (u, w, p) , Steffler and Jin (1993) used a linear profile for u ,

$$u = U + u_1 \left(2 \frac{\eta}{h} - 1 \right), \quad (2.188)$$

and quadratic profiles for w and p ,

$$w = w_b \left(1 - \frac{\eta}{h} \right) + 4w_2 \frac{\eta}{h} \left(1 - \frac{\eta}{h} \right) + w_s \frac{\eta}{h}, \quad (2.189)$$

$$p = (\rho gh + p_1) \left(1 - \frac{\eta}{h} \right) + 4p_2 \frac{\eta}{h} \left(1 - \frac{\eta}{h} \right). \quad (2.190)$$

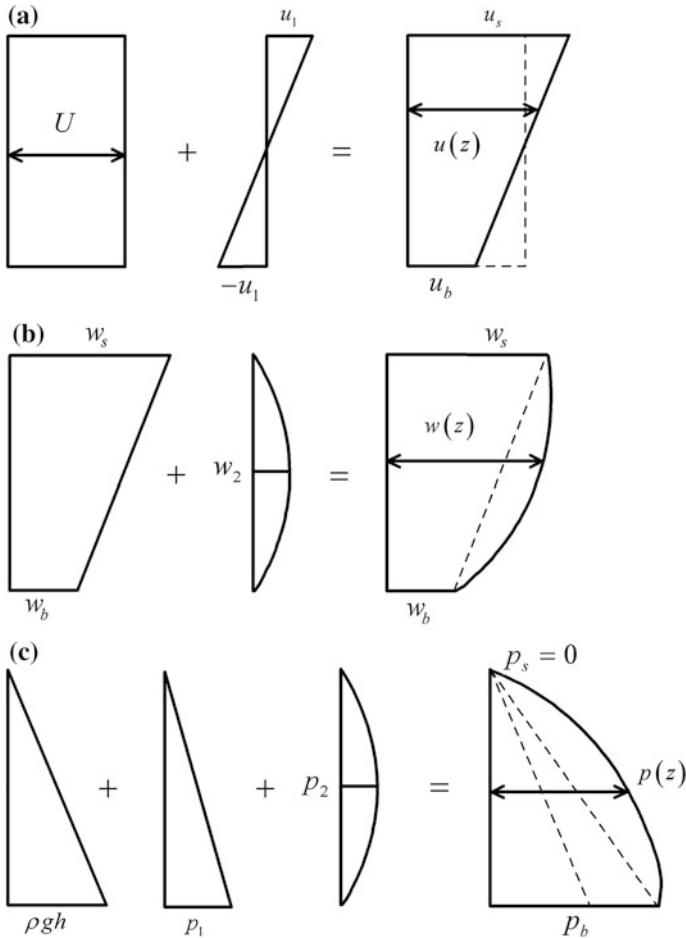


Fig. 2.17 Shape functions used for weighted residual method **a** linear approximation of longitudinal velocity from Eq. (2.188), **b** quadratic distribution of vertical velocity from Eq. (2.189), **c** vertical distribution of pressure from Eq. (2.190)

Here, η is the elevation above the channel bottom, U the vertically averaged horizontal velocity ($= q/h$), u_1 the linearly distributed surface velocity in excess of the mean, w_2 the middepth vertical velocity in excess of the average, p_1 the bed pressure in excess of hydrostatic, and p_2 the midpressure in excess of the pressure average at the bed and surface (Fig. 2.17).

The kinematic boundary conditions are then

$$w_b = \left(\frac{q}{h} - u_1 \right) \frac{\partial z_b}{\partial x}, \quad (2.191)$$

$$w_s = \frac{\partial h}{\partial t} + \left(\frac{q}{h} + u_1 \right) \frac{\partial}{\partial x} (z_b + h). \quad (2.192)$$

The governing system of equations based on these particular functions is given by the continuity equation (Steffler and Jin 1993; Khan and Steffler 1996a, b)

$$\frac{\partial q}{\partial x} + \frac{\partial h}{\partial t} = 0. \quad (2.193)$$

The x -momentum equation, in which τ_b is the bed-shear stress and depth-averaged turbulence stresses are neglected, becomes

$$\frac{\partial q}{\partial t} + \frac{\partial}{\partial x} \left(\frac{q^2}{h} + g \frac{h^2}{2} + \frac{1}{3} h u_1^2 + \frac{1}{2\rho} h p_1 + \frac{2}{3\rho} h p_2 \right) = -g h \frac{\partial z_b}{\partial x} - \frac{p_1}{\rho} \frac{\partial z_b}{\partial x} - \frac{\tau_b}{\rho}, \quad (2.194)$$

and the z -momentum equation is obtained as

$$\frac{\partial}{\partial t} (h\bar{w}) + \frac{\partial}{\partial x} \left[q\bar{w} - \frac{1}{6} (h u_1 \{w_b - w_s\}) \right] = \frac{p_1}{\rho} - \frac{\tau_b}{\rho} \frac{\partial z_b}{\partial x}, \quad (2.195)$$

Based on Eq. (2.189), the depth-averaged vertical velocity \bar{w} is

$$\bar{w} = \frac{w_b + w_s}{2} + \frac{2}{3} w_2. \quad (2.196)$$

Khan and Steffler (1996a, b) further derived the moment equations

$$\frac{1}{4} \frac{\partial h^2}{\partial t} + q \frac{\partial \bar{z}}{\partial x} + \frac{\partial}{\partial x} (h^2 u_1) = h\bar{w}, \quad (2.197)$$

$$\frac{\partial u_1}{\partial t} + \frac{\partial}{\partial x} \left(\frac{q u_1}{h} \right) - \frac{1}{2\rho} \left(\frac{\partial p_1}{\partial x} - \frac{p_1}{h} \frac{\partial h}{\partial x} \right) = -\frac{4p_2}{h\rho} \frac{\partial \bar{z}}{\partial x} + \frac{3}{h} \frac{\tau_b}{\rho}, \quad (2.198)$$

$$\begin{aligned} & \bar{w} \frac{\partial h^2}{\partial t} - \frac{\partial}{\partial t} \left[\frac{h^2}{12} (w_b - w_s) \right] + \left[q\bar{w} - \frac{h u_1}{6} (w_b - w_s) \right] \frac{\partial \bar{z}}{\partial x} \\ & - \frac{\partial}{\partial x} \left[\frac{h q}{12} (w_b - w_s) \right] + \frac{\partial}{\partial x} \left[\frac{h^2 u_1}{10} \left(\frac{w_b + w_s}{3} + \bar{w} \right) \right] - h \bar{w}^2 \\ & - \frac{h \tau_b}{2\rho} \frac{\partial z_b}{\partial x} - \frac{2 h p_2}{3\rho} = 0, \end{aligned} \quad (2.199)$$

in which, based on Eq. (2.189),

$$\overline{w^2} = \bar{w}^2 + \frac{w_b^2}{12} + \frac{w_s^2}{12} - \frac{w_s w_b}{6} + \frac{1}{20} (2\bar{w} - w_b - w_s)^2. \quad (2.200)$$

Equations (2.191)–(2.195) and (2.197)–(2.199) form a system of eight equations for the eight unknowns (h , q , u_1 , w_b , w_s , \bar{w} , p_1 , and p_2). This system was successfully modeled by Khan and Steffler (1996a, b) using the characteristic dissipative Galerkin finite element scheme for flow in hydraulic structures. It may be regarded as a higher-order Boussinesq-type model with increased order of vertical resolution. If $u_1 = w_2 = p_2 = 0$, then the standard Boussinesq equations are recovered.

References

- Abbott, M. B. (1979). *Computational hydraulics: Elements of the theory of free surface flows*. London: Pitman.
- Ancey, C. (2010). Stochastic modelling in sediment dynamics: Exner equation for planar incipient bed load transport conditions. *Journal of Geophysical Research*, 115, F00A11. doi:[10.1029/2009JF001260](https://doi.org/10.1029/2009JF001260)
- Andreotti, B., Forterre, Y., & Pouliquen, O. (2013). *Granular media: Between fluid and solid*. Cambridge: Cambridge University Press.
- Antunes do Carmo, J. S., Santos, F. J., & Almeida, A. B. (1993). Numerical solution of the generalized Serre equations with the MacCormack finite difference scheme. *International Journal for Numerical Methods in Fluids*, 16(8), 725–738.
- ASCE Task Committee on flow and transport over dunes. (2002). Flow and transport over dunes. *Journal of Hydraulic Engineering*, 128(8), 726–728.
- Bagnold, R. A. (1973). The nature of saltation and of ‘bed-load’ transport in water. *Proceedings of the Royal Society of London. Series A*, 332, 473–504.
- Barthelemy, E. (2004). Nonlinear shallow water theories for coastal waters. *Surveys In Geophysics*, 25, 315–337.
- Basco, D. R. (1983). Computation of rapidly varied, unsteady free surface flow. *Water Resources Investigation Report 83-4284*. Reston VA: US Geological Survey.
- Benjamin, T. B., & Lighthill, M. J. (1954). On cnoidal waves and bores. *Proceedings of the Royal Society of London. Series A*, 224, 448–460.
- Berger, R. C., & Carey, G. F. (1998a). Free-surface flow over curved surfaces. Part I: Perturbation analysis. *International Journal for Numerical Methods in Fluids*, 28, 191–200.
- Berger, R. C., & Carey, G. F. (1998b). Free-surface flow over curved surfaces. Part II: Computational model. *International Journal for Numerical Methods in Fluids*, 28, 201–213.
- Bonneton, P., Barthelemy, E., Chazel, F., Cienfuegos, R., Lannes, D., Marche, F., et al. (2011). Recent advances in Serre-Green Naghdi modelling for wave transformation, breaking and runoff processes. *The European Journal of Mechanics—B/Fluids*, 30, 589–597.
- Bose, S. K., & Dey, S. (2007). Curvilinear flow profiles based on Reynolds averaging. *Journal of Hydraulic Engineering*, 133(9), 1074–1079.
- Bose, S. K., & Dey, S. (2009). Reynolds averaged theory of turbulent shear flows over undulating beds and formation of sand waves. *Physical Review E*, 80(3), 036304-1–036304-9.
- Boussinesq, J. (1872). Théorie des ondes et des remous qui se propagent le long d’un canal rectangulaire horizontal, en communiquant au liquide contenu dans ce canal des vitesses

- sensiblement pareilles de la surface au fond (Theory of waves and disturbances propagating along a rectangular horizontal channel, generating nearly uniform velocities from the surface to the bottom). *Journal de Mathématiques Pures et Appliquées* (Série 2), 17, 55–108 (in French).
- Boussinesq, J. (1877). Essai sur la théorie des eaux courantes (Essay on the theory of water flow). *Mémoires présentés par divers savants à l'Académie des Sciences, Paris*, 23, 1–680. (in French).
- Brocchini, M. (2013). A reasoned overview on Boussinesq-type models: the interplay between physics, mathematics and numerics. *Proceedings of the Royal Society of London. Series A*, 469, 20130496.
- Buffington, J. M., & Montgomery, D. R. (1997). A systematic analysis of eight decades of incipient motion studies, with special reference to gravel-bedded rivers. *Water Resources Research*, 33(8), 1993–2029.
- Cantero-Chinchilla, F. N., Castro-Orgaz, O., Dey, S., & Ayuso, J. L. (2016a). Nonhydrostatic dam break flows I: Physical equations and numerical schemes. *Journal of Hydraulic Engineering*, 142(12), 04016068.
- Cantero-Chinchilla, F. N., Castro-Orgaz, O., Dey, S., & Ayuso, J. L. (2016b). Nonhydrostatic dam break flows II: One-dimensional depth-averaged modelling for movable bed flows. *Journal of Hydraulic Engineering*, 142(12), 0416069.
- Carter, J. D., & Cienfuegos, R. (2011). The kinematics and stability of solitary and cnoidal wave solutions of the Serre equations. *The European Journal of Mechanics—B/Fluids*, 30(5–6), 259–268.
- Castro-Orgaz, O., Giráldez, J. V., & Mateos, L. (2013). Second-order shallow flow equation for anisotropic aquifers. *Journal of Hydrology*, 501, 183–185.
- Castro-Orgaz, O., Giráldez, J. V., & Robinson, N. (2012). Second order two-dimensional solution for the drainage of recharge based on Picard's iteration technique: A generalized Dupuit-Forchheimer equation. *Water Resources Research*, 48, W06516. doi:[10.1029/2011WR011751](https://doi.org/10.1029/2011WR011751)
- Castro-Orgaz, O., & Hager, W. H. (2009). Curved streamline transitional flow from mild to steep slopes. *Journal of Hydraulic Research*, 47(5), 574–584.
- Castro-Orgaz, O., & Hager, W. H. (2011a). Joseph Boussinesq and his theory of water flow in open channels. *Journal of Hydraulic Research*, 49(5), 569–577.
- Castro-Orgaz, O., & Hager, W. H. (2011b). Turbulent near-critical open channel flow: Serre's similarity theory. *Journal of Hydraulic Engineering*, 137(5), 497–503.
- Castro-Orgaz, O., & Hager, W. H. (2011c). Observations on undular jump in movable bed. *Journal of Hydraulic Engineering*, 49(5), 689–692.
- Castro-Orgaz, O., Hutter, K., Giráldez, J. V., & Hager, W. H. (2015). Non-hydrostatic granular flow over 3D terrain: New Boussinesq-type gravity waves? *Journal of Geophysical Research—Earth Surface*, 120(1), 1–28.
- Chanson, H. (2000). Boundary shear stress measurements in undular flows: Application to standing wave bed forms. *Water Resources Research*, 36(10), 3063–3076.
- Chaudhry, M. H. (2008). *Open-channel flow* (2nd ed.). Berlin: Springer.
- Chen, Q. (2006). Fully nonlinear Boussinesq-type equations for waves and currents over porous beds. *The Journal of Engineering Mechanics*, 132(2), 220–230.
- Chen, Q., Kirby, J. T., Dalrymple, R. A., Kennedy, A. B., & Haller, C. M. (1999). Boussinesq modeling of a rip current system. *Journal of Geophysical Research*, 104(C9), 20617–20637.
- Chen, Q., Kirby, J. T., Dalrymple, R. A., Shi, F., & Thornton, E. B. (2003). Boussinesq modeling of longshore currents. *Journal of Geophysical Research*, 108(C11), 3362–3380.
- Chen, Y., & Liu, P. L. F. (1995). Modified Boussinesq equations and associated parabolic models for water wave propagation. *Journal of Fluid Mechanics*, 288, 351–381.
- Chow, V. T. (1959). *Open channel hydraulics*. New York: McGraw-Hill.
- Cienfuegos, R., Barthélemy, E., & Bonneton, P. (2006). A fourth-order compact finite volume scheme for fully nonlinear and weakly dispersive Boussinesq-type equations. Part I: Model development and analysis. *International Journal for Numerical Methods in Fluids*, 51(11), 1217–1253.

- De Saint-Venant, A. B. (1871). Théorie du mouvement non permanent des eaux, avec application aux crues des rivières et à l'introduction des marées dans leur lit (Theory of unsteady water movement, applied to floods in rivers and the effect of tidal flows). *Comptes Rendus de l'Académie des Sciences*, 73, 147–154; 73, 237–240 (in French).
- Denlinger, R. P., & Iverson, R. M. (2004). Granular avalanches across irregular three-dimensional terrain: 1. Theory and computation. *Journal of Geophysical Research*, 109(F1), F01014. doi:[10.1029/2003JF000085](https://doi.org/10.1029/2003JF000085)
- Denlinger, R. P., & O'Connell, D. R. H. (2008). Computing nonhydrostatic shallow-water flow over steep terrain. *Journal of Hydraulic Engineering*, 134(11), 1590–1602.
- Dewals, B. J., Erpicum, S., Archambeau, P., Detrembleur, S., & Piroton, M. (2006). Depth-integrated flow modelling taking into account bottom curvature. *Journal of Hydraulic Research*, 44(6), 785–795.
- Dey, S. (2014). *Fluvial hydrodynamics: Hydrodynamic and sediment transport phenomena*. Berlin: Springer.
- Dias, F., & Milewski, P. (2010). On the fully non-linear shallow-water generalized Serre equations. *Physics Letters A*, 374, 1049–1053.
- Dressler, R. F. (1978). New nonlinear shallow flow equations with curvature. *Journal of Hydraulic Research*, 16(3), 205–222.
- Einstein, H. A. (1950). The bed-load function for sediment transportation in open channel flows. *USDA Technical Bulletin*, 1026. Washington D.C.
- Engelund, F., & Fredsoe, J. (1976). A sediment transport model for straight alluvial channels. *Nordic Hydrology*, 7(5), 293–306.
- Engelund, F., & Fredsoe, J. (1982). Sediment ripples and dunes. *Annual Review of Fluid Mechanics*, 14, 13–37.
- Engelund, F., & Hansen, E. (1966). Investigations of flow in alluvial streams. *Hydraulic Laboratory Bulletin* 9. Copenhagen: Technical University of Denmark.
- Erduran, K. S., Ilic, S., & Kutija, V. (2005). Hybrid finite-volume finite-difference scheme for the solution of Boussinesq equations. *International Journal for Numerical Methods in Engineering*, 49(11), 1213–1232.
- Fawer, C. (1937). Etude de quelques écoulements permanents à filets courbes (Study of some steady flows with curved streamlines). *Thesis*, Université de Lausanne, La Concorde, Lausanne, Switzerland (in French).
- Fenton, J. D. (1996). Channel flow over curved boundaries and a new hydraulic theory. *Proceedings of the 10th IAHR APD Congress*, Langkawi, Malaysia (pp. 266–273).
- Fenton, J. D., & Zerihun, Y. T. (2007). A Boussinesq approximation for open channel flow. *Proceedings of the 32th IAHR Congress*, Venice, Italy, published on CD.
- Friedrichs, K. O. (1948). On the derivation of the shallow water theory. *Communications on Pure and Applied Mathematics*, 1(1), 81–87.
- Furbish, D. J., Haff, P. K., Roseberry, J. C., & Schmeeckle, M. W. (2012). A probabilistic description of the bed load sediment flux: 1. Theory. *Journal of Geophysical Research*, 117, F03031. doi:[10.1029/2012JF002352](https://doi.org/10.1029/2012JF002352)
- García, M. H. (2008). Sedimentation engineering: Processes, measurements, modeling, and practice. *ASCE Manual of practice*, 110. Reston, VA.
- Graf, W. H., & Altinakar, M. S. (1996). *Hydraulique fluviale: Écoulement non-permanent et phénomènes de transport* (Fluvial hydraulics: Unsteady flow and transport phenomena). Paris: Eyrolles (in French).
- Green, A. E., & Naghdi, P. M. (1976). A derivation of equations for wave propagation in water of variable depth. *Journal of Fluid Mechanics*, 78, 237–246.
- Guinot, V. (2003). Riemann solvers and boundary conditions for two dimensional shallow water simulations. *International Journal for Numerical Methods in Engineering*, 41(11), 1191–1219.
- Hager, W. H. (1983). Hydraulics of plane free overfall. *Journal of Hydraulic Engineering*, 109(12), 1683–1697.

- Hager, W. H., & Hager, K. (1985). Streamline curvature effects in distribution channels. *Proceedings of IME*, 199(3), 165–172.
- Hager, W. H., & Hutter, K. (1984a). Approximate treatment of plane channel flow. *Acta Mechanica*, 51(3–4), 31–48.
- Hager, W. H., & Hutter, K. (1984b). On pseudo-uniform flow in open channel hydraulics. *Acta Mechanica*, 53(3–4), 183–200.
- Henderson, F. M. (1966). *Open channel flow*. New York: MacMillan.
- Hervouet, J. M. (2007). *Hydrodynamics of free surface flows: Modelling with the finite element method*. New York: Wiley & Sons.
- Hosoda, T., & Tada, A. (1994). Free surface profile analysis on open channel flow by means of 1-D basic equations with effect of vertical acceleration. *Annual Journal of Hydraulics Engineering. JSCE*, 38, 457–462 (in Japanese).
- Hutter, K., & Castro-Orgaz, O. (2016). Non-hydrostatic free surface flows: Saint Venant versus Boussinesq depth integrated dynamic equations for river and granular flows (Chapter 17). In *Continuous media with microstructure 2* (pp. 245–265). Berlin: Springer.
- Hutter, K., & Jöhnik, K. (2004). *Continuum methods of physical modeling: Continuum mechanics, dimensional analysis, turbulence*. Berlin: Springer.
- Hutter, K., & Savage, S. B. (1988). Avalanche dynamics: The motion of a finite mass of gravel down a mountain side. *Proceedings of the 5th International Symposium on Landslides*, Lausanne (pp. 691–697).
- Hutter, K., & Wang, Y. (2016). *Fluid and thermodynamics 1: Basic fluid mechanics, 2: Advanced fluid mechanics and thermodynamics*. Berlin: Springer.
- Iverson, R. M. (1997). The physics of debris flows. *Reviews of Geophysics*, 35(3), 245–296.
- Iverson, R. M. (2005). Debris-flow mechanics. In M. Jakob & O. Hungr (Eds.), *Debris flow hazards and related phenomena* (pp. 105–134). Heidelberg: Springer.
- Iwasa, Y. (1955). Undular jump and its limiting conditions for existence. *Proceedings of the 5th Japan national congress in applied mechanics II*, 14, 315–319.
- Iwasa, Y. (1956). Analytical considerations on cnoidal and solitary waves. *Transactions of Japan Society of Civil Engineers*, 32, 43–49.
- Iwasa, Y., & Kennedy, J. F. (1968). Free surface shear flow over a wavy bed. *Journal of the Hydraulics Division*, 94(HY2), 431–454.
- Jain, S. C. (2001). *Open channel flow*. New York: Wiley & Sons.
- Kennedy, J. F. (1963). The mechanics of dunes and antidunes in erodible-bed channels. *Journal of Fluid Mechanics*, 16, 521–544.
- Kennedy, A. B., Chen, Q., Kirby, J. T., & Dalrymple, R. A. (2000). Boussinesq modeling of wave transformation, breaking, and run-up. Part I: 1D. *Journal of Waterway Port Coastal and Ocean Engineering*, 126(1), 39–47.
- Khan, A. A., & Lai, W. (2014). *Modelling shallow water flows using the discontinuous Galerkin method*. London: CRC Press, Taylor and Francis.
- Khan, A. A., & Steffler, P. M. (1996a). Modelling overfalls using vertically averaged and moment equations. *Journal of Hydraulic Engineering*, 122(7), 397–402.
- Khan, A. A., & Steffler, P. M. (1996b). Vertically averaged and moment equations model for flow over curved beds. *Journal of Hydraulic Engineering*, 122(1), 3–9.
- Kim, D.-H., & Lynett, P. J. (2011). Dispersive and nonhydrostatic pressure effects at the front of surge. *Journal of Hydraulic Engineering*, 137(7), 754–765.
- Kim, D.-H., Lynett, P. J., & Socolofsky, S. (2009). A depth-integrated model for weakly dispersive, turbulent, and rotational fluid flows. *Ocean Modelling*, 27(3–4), 198–214.
- Lajeunesse, E., Malverti, L., & Charru, F. (2010). Bed load transport in turbulent flow at the grain scale: Experiments and modelling. *Journal of Geophysical Research*, 115, F04001. doi:[10.1029/2009JF001628](https://doi.org/10.1029/2009JF001628)
- Lannes, D., & Bonneton, P. (2009). Derivation of asymptotic two-dimensional time-dependent equations for surface water wave propagation. *Physics of Fluids*, 21(1), 016601, 9 pp.
- LeVeque, R. J. (2002). *Finite volume methods for hyperbolic problems*. Cambridge: Cambridge University Press.

- Liggett, J. A. (1994). *Fluid mechanics*. New York: McGraw-Hill.
- Lynett, P. J. (2006). Wave breaking effects in depth-integrated models. *Coastal Engineering*, 53(4), 325–333.
- Lynett, P., Wu, T. R., & Liu, P. L.-F. (2002). Modeling wave runup with depth-integrated equations. *Coastal Engineering*, 46(2), 89–107.
- Ma, G., Fengyang, S., & Kirby, J. T. (2012). Shock-capturing non-hydrostatic model for fully dispersive surface wave processes. *Ocean Modelling*, 43–44, 22–35.
- Madsen, P. A., & Schäffer, H. A. (1998). Higher-order Boussinesq-type equations for surface gravity waves: Derivation and analysis. *Philosophical Transactions of the Royal Society of London. Series A*, 356, 3123–3184.
- Madsen, P. A., Sorensen, O. R., & Schäffer, H. A. (1997). Surf zone dynamics simulated by a Boussinesq type model. I. Model description and cross-shore motion of regular waves. *Coastal Engineering*, 32(4), 255–287.
- Mandrup-Andersen, V. (1975). Transition from subcritical to supercritical flow. *Journal of Hydraulic Research*, 13(3), 227–238.
- Mandrup-Andersen, V. (1978). Undular hydraulic jump. *Journal of the Hydraulics Division, ASCE* 104(HY8), 1185–1188; *Discussion*, 105(HY9), 1208–1211.
- Marchi, E. (1963). Contributo allo studio del risalto ondulato (Contribution to the study of the undular hydraulic jump). *G. Genio Civile*, 101(9), 466–476. (in Italian).
- Marchi, E. (1992). The nappe profile of a free overfall. *Rendiconti Lincei Matematica e Applicazioni Serie 9*, 3(2), 131–140.
- Marchi, E. (1993). On the free overfall. *Journal of Hydraulic Research*, 31(6), 777–790; 32(5), 794–796.
- Matthew, G. D. (1963). On the influence of curvature, surface tension and viscosity on flow over round-crested weirs. *Proceedings of ICE* 25, 511–524; 28, 557–569.
- Matthew, G. D. (1991). Higher order one-dimensional equations of potential flow in open channels. *Proceedings of ICE*, 91(3), 187–201.
- Mei, C. C. (1983). *The applied dynamics of ocean surface waves*. New York: John Wiley.
- Meyer-Peter, E., & Müller, R. (1948). Formulas for bed load transport. *Proceedings of the 2nd International IAHR Meeting, Stockholm*, 26, 5–24.
- Mignot, E., & Cienfuegos, R. (2008). On the application of a Boussinesq model to river flows including shocks. *Coastal Engineering*, 56(1), 23–31.
- Mohapatra, P. K., & Chaudhry, M. H. (2004). Numerical solution of Boussinesq equations to simulate dam-break flows. *Journal of Hydraulic Engineering*, 130(2), 156–159.
- Molls, T., & Chaudhry, M. H. (1995). Depth averaged open channel flow model. *Journal of Hydraulic Engineering*, 121(6), 453–465.
- Montes, J. S. (1986). A study of the undular jump profile. *Proceedings of the 9th Australasian Fluid Mechanics Conference, Auckland* (pp. 148–151).
- Montes, J. S. (1998). *Hydraulics of open channel flow*. Reston, VA: ASCE Press.
- Musumeci, R. E., Svendsen, I. A., & Veeramony, J. (2005). The flow in the surf zone: A fully nonlinear Boussinesq-type of approach. *Coastal Engineering*, 52(7), 565–598.
- Nwogu, O. (1993). Alternative form of Boussinesq equations for nearshore wave propagation. *Journal of Waterway Port Coastal and Ocean Engineering*, 119(6), 618–638.
- Onda, S., & Hosoda, T. (2004). Numerical simulation of the development process of dunes and flow resistance. In *Proceedings of River Flow 2004* (245–252). London: T&F.
- Parker, G. (1979). Hydraulic geometry of active gravel rivers. *Journal of Hydraulics Division, ASCE*, 105(9), 1185–1201.
- Peregrine, D. H. (1966). Calculations of the development of an undular bore. *Journal of Fluid Mechanics*, 25(2), 321–330.
- Peregrine, D. H. (1967). Long waves on a beach. *Journal of Fluid Mechanics*, 27(5), 815–827.

- Peregrine, D. H. (1972). Equations for water waves and the approximations behind them. In R. E. Meyer (Ed.), *Waves on beaches and resulting sediment transport* (pp. 95–122). San Diego, CA: Academic Press.
- Pudasaini, S. P., & Hutter, K. (2007). *Avalanche dynamics*. Berlin: Springer.
- Roache, P. J. (1976). *Computational fluid dynamics*. Albuquerque, NM: Hermosa Publishers.
- Rodi, W. (1980). *Turbulence models and their application in hydraulics: A state-of-the-art review*. Dordrecht: IAHR.
- Savage, S. B., & Hutter, K. (1989). The motion of a finite mass of granular material down a rough incline. *Journal of Fluid Mechanics*, 199, 177–215.
- Savage, S. B., & Hutter, K. (1991). The dynamics of avalanches of granular materials from initiation to runout I: Analysis. *Acta Mechanica*, 86(1–4), 201–223.
- Schmocker, L. (2011). Hydraulics of dike breaching. *Dissertation ETH 19983*. Zürich, Switzerland: ETH Zurich.
- Seabra-Santos, F. J., Renouard, D. P., & Temperville, A. M. (1987). Numerical and experimental study of the transformation of a solitary wave over a shelf or isolated obstacle. *Journal of Fluid Mechanics*, 176, 117–134.
- Serre, F. (1953). Contribution à l'étude des écoulements permanents et variables dans les canaux (Contribution to the study of steady and unsteady channel flows). *La Houille Blanche*, 8(6–7), 374–388; 8(12), 830–887 (in French).
- Sivakumaran, N. S., & Dressler, R. F. (1989). Unsteady density-current equations for highly curved terrain. *Journal of the Atmospheric Sciences*, 46(20), 3192–3201.
- Sivakumaran, N. S., Tingsanchali, T., & Hosking, R. J. (1983). Steady shallow flow over curved beds. *Journal of Fluid Mechanics*, 128, 469–487.
- Soares-Frazão, S., & Guinot, V. (2008). A second-order semi-implicit hybrid scheme for one-dimensional Boussinesq-type waves in rectangular channels. *The International Journal for Numerical Methods in Fluids*, 58(3), 237–261.
- Soares-Frazão, S., & Zech, Y. (2002). Undular bores and secondary waves: Experiments and hybrid finite-volume modelling. *Journal of Hydraulic Research*, 40(1), 33–43.
- Stansby, P. K. (2003). Solitary wave run up and overtopping by a semi-implicit finite-volume shallow-water Boussinesq model. *Journal of Hydraulic Research*, 41(6), 639–647.
- Stansby, P. K., & Zhou, J. G. (1998). Shallow-water flow solver with non-hydrostatic pressure: 2D vertical plane problems. *The International Journal for Numerical Methods in Fluids*, 28(3), 541–563.
- Steffler, P. M., & Jin, Y. C. (1993). Depth-averaged and moment equations for moderately shallow free surface flow. *Journal of Hydraulic Research*, 31(1), 5–17.
- Su, C. H., & Gardner, C. S. (1969). KDV equation and generalizations. Part III. Derivation of Korteweg-de Vries equation and Burgers equation. *Journal of Mathematical Physics*, 10(3), 536–539.
- Toro, E. F. (1997). *Riemann solvers and numerical methods for fluid dynamics*. Berlin: Springer.
- Toro, E. F. (2001). *Shock-capturing methods for free-surface shallow flows*. New York: Wiley.
- Vreugdenhil, C. B. (1994). *Numerical methods for shallow water flow*. Dordrecht NL: Kluwer.
- Wei, G., & Kirby, J. T. (1995). Time-dependent numerical code for extended Boussinesq equations. *Journal of Waterway Port Coastal and Ocean Engineering*, 121(5), 251–261.
- Wei, G., Kirby, J. T., Grilli, S. T., & Subramanya, R. (1995). A fully nonlinear Boussinesq model for surface waves 1: Highly nonlinear unsteady waves. *Journal of Fluid Mechanics*, 294, 71–92.
- Wiberg, P., & Smith, J. D. (1989). Model for calculating bed load transport of sediment. *Journal of Hydraulic Engineering*, 115(1), 101–123.
- Wieland, M., Gray, J. M. N. T., & Hutter, K. (1999). Channelised free surface flow of cohesionless granular avalanche in a chute with shallow lateral curvature. *Journal of Fluid Mechanics*, 392, 73–100.
- Yalin, M. S. (1977). *Mechanics of sediment transport*. Oxford: Pergamon.

- Yen, B. C. (1973). Open-channel flow equations revisited. *Journal of the Engineering Mechanics Division, ASCE*, 99(EM5), 979–1009.
- Zerihun, Y., & Fenton, J. (2006). One-dimensional simulation model for steady transcritical free surface flows at short length transitions. *Advances in Water Resources*, 29(11), 1598–1607.
- Zerihun, Y., & Fenton, J. (2007). A Boussinesq-type model for flow over trapezoidal profile weirs. *Journal of Hydraulic Research*, 45(4), 519–528.
- Zhu, D. Z., & Lawrence, G. A. (1998). Non-hydrostatic effects in layered shallow water flows. *Journal of Fluid Mechanics*, 355, 1–16.

Non-Hydrostatic Free Surface Flows

Castro-Orgaz, O.; HAGER, W.H.

2017, XVI, 696 p. 230 illus., 17 illus. in color., Hardcover

ISBN: 978-3-319-47969-9